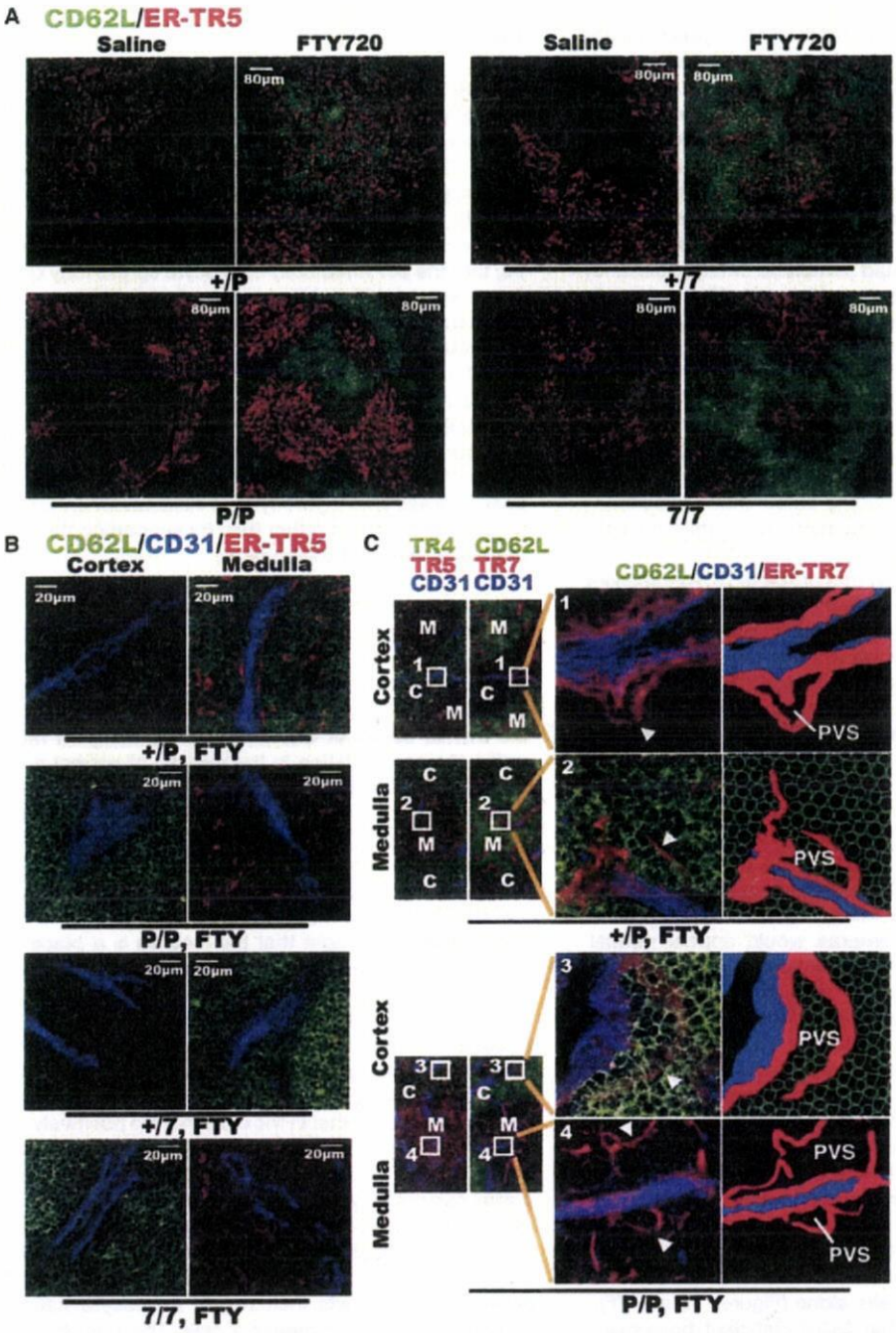

Figure 3. FTY720-Mediated Accumulation of Mature Thymocytes in the Thymic Cortex of CCR7- or CCR7L-Deficient Mice

Frozen sections of the thymus from indicated mice were two-color or three-color stained for CD62L (green) and mTEC-specific ER-TR5 (red) (A); CD62L (green), CD31 (blue), and ER-TR5 (red) (B); ER-TR4 (green), CD31 (blue), and ER-TR5 (red) (C); or CD62L (green), CD31 (blue), and ER-TR7 (red) (C), as indicated. The cortex and the medulla in (B) were identified by staining of the adjacent sections with cTEC-specific ER-TR4 and mTEC-specific ER-TR5. The high magnification images in (B) show that in the cortex of FTY720-mediated CCR7L-deficient mice (P/P) and CCR7-deficient mice (7/7) and in the medulla of FTY720-mediated control mice (+/P and +/7), there are the areas where many CD62L^{high} thymocytes were accumulated around CD31^{+} endothelial vessels. It should be noted that low-magnification images of the cortex in the FTY720-treated mutant mice (P/P and 7/7) and of the medulla in the FTY720-treated control mice (+/P and +/7) show that not all areas in the cortex are uniformly filled with CD62L^{high} thymocytes and that there are also the cortical areas where only a few CD62L^{high} thymocytes were found (A). On the other hand, no or very few CD62L^{high} thymocytes were found in the medulla of FTY720-mediated CCR7- or CCR7L-deficient mice (P/P and 7/7) and in the cortex of FTY720-mediated control mice (+/P and +/7) in low-magnification as well as in high-magnification images (A and B).

(C) Serial sections were stained as indicated. The cortex (C) and the medulla (M) were identified by ER-TR4 and ER-TR5. The perivascular space (PVS) was identified as the areas surrounded by CD31^{+} endothelial and ER-TR7^{+} mesenchymal cells. High-magnification images of boxes 1, 2, 3,

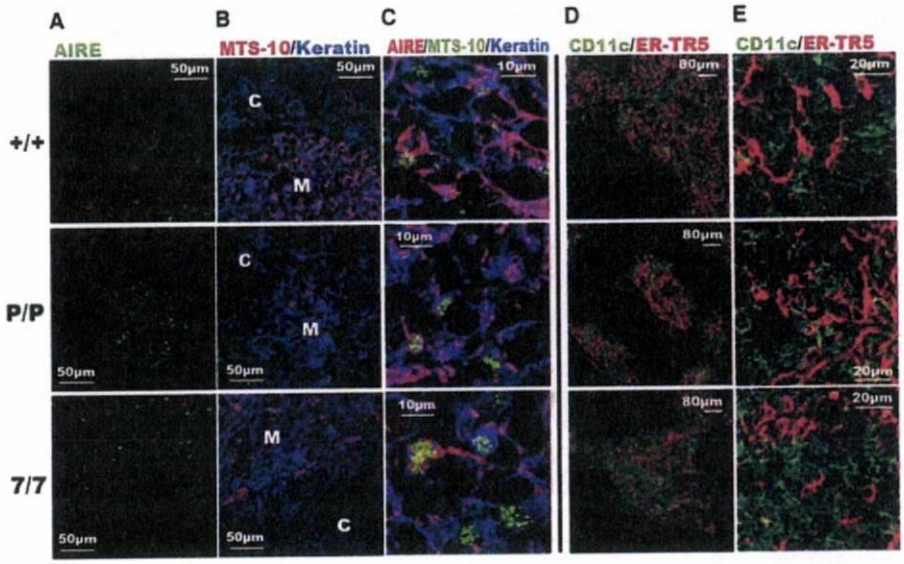

Figure 4. Intrathymic Distribution of AIRE-Expressing Cells and DCs in CCR7- or CCR7L-Deficient Mice

(A–C) Thymus sections from B6 (+/+), *plt/plt* (P/P), and CCR7-deficient (7/7) adult mice were stained with anti-AIRE (green), anti-keratin (blue), and mTEC-specific MTS-10 (red) antibodies. Cortex (C) and medulla (M) were identified with MTS-10 staining (B). High-magnification images from the three-color staining in (C) show that AIRE, keratin, and the MTS-10 determinant in the mutant mice as well as in the control mice are expressed in single mTEC, although AIRE is selectively localized in the nuclei whereas keratin and MTS-10 determinants are predominantly localized at the cytoplasm and the plasma membrane, respectively.

(D and E) Thymus sections from indicated mice were also stained for CD11c (green) and ER-TR5 (red).

Shown are representative results of more than three independent analyses.

the mutant mice may represent mature thymocytes that will eventually be exported from the thymus. Nevertheless, it is possible that some mature thymocytes in CCR7- or CCR7L-deficient mice may egress from the thymus through the medullary and/or cortico-medullary junction areas.

Perhaps, however, it is more tempting to speculate that the minor fraction of mature thymocytes found in the medulla of CCR7- or CCR7L-deficient mice may contribute to the crosstalk signals to induce the generation of AIRE$^+$ mTEC in the medullary area. It was previously shown that the generation of mature SP thymocytes is essential for the development of the medullary epithelial architecture (van Ewijk et al., 1994). On the other hand, CCR7- or CCR7L-deficient mice generate the thymus with a small but distinct medullary region (Ueno et al., 2004) that contains AIRE$^+$ mTEC as well as DCs (Figure 4), even though the generation of UEA-1$^+$ clusters in the medulla is impaired (Ueno et al., 2004; also shown in Figure 7 of this study). Thus, it is possible that the CCR7-independent migration into the medulla by a small fraction of mature thymocytes may play a role in the development of TEC precursor cells to generate AIRE$^+$ mTEC and the localization of DCs in the medulla.

The perivascular space in the postnatal thymus is distributed around the venules and some arterioles and is enriched in the medulla and the cortico-medullary junction (Ushiki, 1986; Kato, 1997). However, the perivascular space is also found within the cortex in normal animals (Ushiki, 1986; Kato, 1997; F.S. and Y.T., unpublished data). It has been speculated that the perivascular space is a route for T cell egress from the thymus parenchyma to the circulation (Ushiki, 1986; Kato, 1997). Indeed, our results show that the FTY720-mediated blockade of the S1P-dependent egress results in the accumulation of mature thymocytes even in the perivascular space that is localized in the medulla of normal mice (Figure 3C), supporting the possibility that the medullary perivascular space is a route for the S1P-dependent T cell egress from the thymus in normal mice. Interestingly, however, in mice deficient in CCR7 or CCR7L, the FTY720 treatment accumulates most mature thymocytes in the cortex rather than in the medulla. The accumulation in these mutant mice is detected even in the perivascular space within the cortex (Figure 3C). These results not only reinforce the possibility that the cortex is capable of supporting T cell export, but also support the possibility that the perivascular space within the cortex can serve as a route for the S1P-dependent egress of mature thymocytes. Thus, our results suggest that the cortex-to-medulla migration of developing thymocytes may not be required for the further maturation of thymocytes or for the export of mature thymocytes.

The possibility that similar to the medulla, the cortex can support the generation and export of mature SP thymocytes prompts us to question why the maturation

and 4 show the representative areas of cortical PVS in +/P mice, medullary PVS in +/P mice, cortical PVS in P/P mice, and medullary PVS in P/P mice, respectively. Arrows in the high-magnification images (1–4) indicate the representative PVSs, which are also schematically depicted in the right panels. Shown are representative results of more than ten independent analyses.

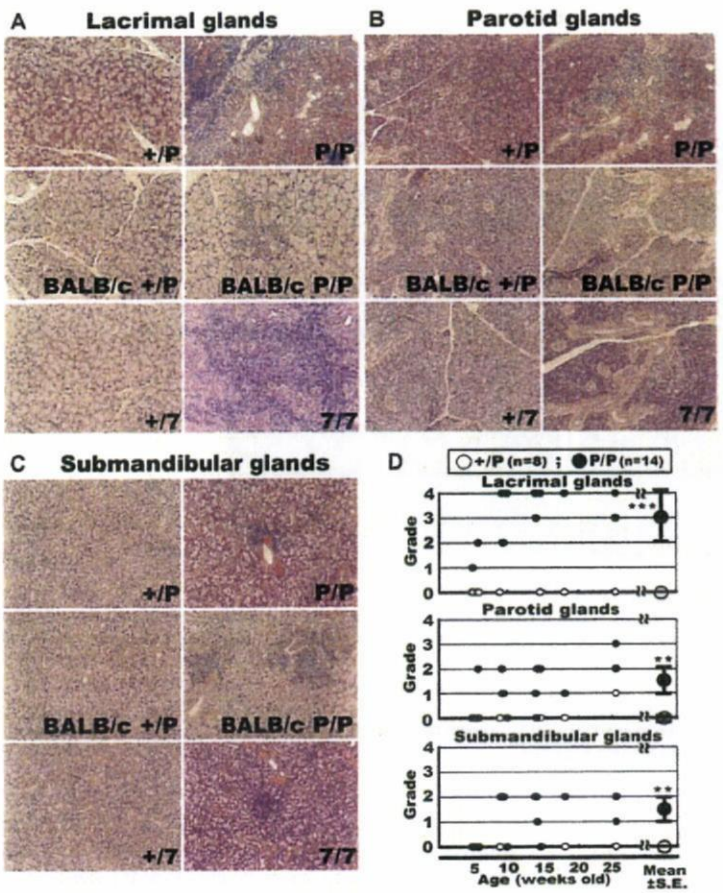

Figure 5. CCR7- or CCR7L-Deficient Mice Exhibit Lymphocyte Infiltration in Lacrimal and Salivary Glands with Tissue Damage

Representative hematoxylin- and eosin-stained tissue sections of lacrimal glands (A), parotid glands (B), and submandibular glands (C) from CCR7L-deficient mice (*plt/plt*, P/P), CCR7-deficient mice (7/7), and their heterozygous control mice (+/P and +/7) are shown. Where indicated, the sections were obtained from *plt/plt* (P/P) and *+/plt* (+/P) mice of BALB/c background.

(D) Histological grading of inflammatory lesions in *plt/plt* (P/P; closed circles) and *+/plt* (+/P; open circles) mice at the indicated age was performed as described in the Experimental Procedures. Double asterisk indicates $p < 0.005$ and triple asterisk indicates $p < 0.0005$ by the Mann-Whitney test.

and export of SP thymocytes in normal mice occur predominantly in the medulla rather than in the cortex. In agreement with previous reports (Matloubian et al., 2004; Allende et al., 2004), our results show that S1P1, the receptor for S1P in T cells, is expressed predominantly by $CD62L^{high}CD69^{low}$ mature SP thymocytes rather than by the less immature thymocytes, including DN, DP, and $CD62L^{low}CD69^{high}$ SP cells. It is therefore likely that most thymocytes, including the DN and DP immature cortical thymocytes as well as the $CD62L^{low}CD69^{high}$ semimature SP thymocytes, are not attracted to S1P, even though neighboring vasculatures in the cortex may supply a gradient of S1P toward the circulation. On the other hand, positively selected DP thymocytes begin expressing a low level of CCR7 (Ueno et al., 2004), and CCR7 is clearly expressed on the positively selected thymocytes at the semimature $CD62L^{low}CD69^{high}$ SP thymocyte stage (Figure 1). Thus, it is likely that in normal mice, positively selected thymocytes in the cortex are attracted to CCR7L, which is predominantly expressed in the medulla, but not attracted to S1P, which penetrates from the vasculature even in the cortex, so that the majority of the positively selected thymocytes are attracted to and accumulated in the medulla. Upon completion of thymocyte differentiation, the S1P1-expressing mature SP thymocytes may be exported to the circulation via the perivascular space within either the medulla or the cortex.

It is also interesting to note that $CD62L^{+}$ cells are sparsely found in the cortex, rather than in the medulla, of the normal untreated mice (Figure 3A), in agreement with previous reports (Reichert et al., 1984; Fink et al., 1985). It was reported that $CD62L^{+}$ cortical thymocytes in normal untreated mice are generated before birth and contain immature DN cells (Reichert et al., 1986a, 1986b), whereas $CD62L^{high}$ mature SP thymocytes are rare in untreated mice and are increased in number upon FTY720 treatment within the medulla of normal mice (Figures 2C and 3A). The developmental status, particularly the significance in thymocyte export, of the $CD62L^{+}$ cells visualized in the cortex of normal untreated mice is still unclear and warrants further analysis.

Medulla Migration and Central Tolerance

Our results show that CCR7- or CCR7L-deficient mice exhibit autoimmune dacryoadenitis and sialadenitis with antibody deposit and tissue damage and that this exocrinopathy is reproduced in lymphocyte-lacking RAG2-deficient mice that are transferred with thymocytes from CCR7L-deficient mice. These results indicate that the thymocytes that are generated without CCR7 signals do not fully establish self-tolerance to the organs, such as lacrimal and salivary glands. Because thymocytes that develop in CCR7- or CCR7L-deficient mice fail to accumulate in the medulla and may be exported directly from the cortex, and because $AIRE^{+}$ cells in the

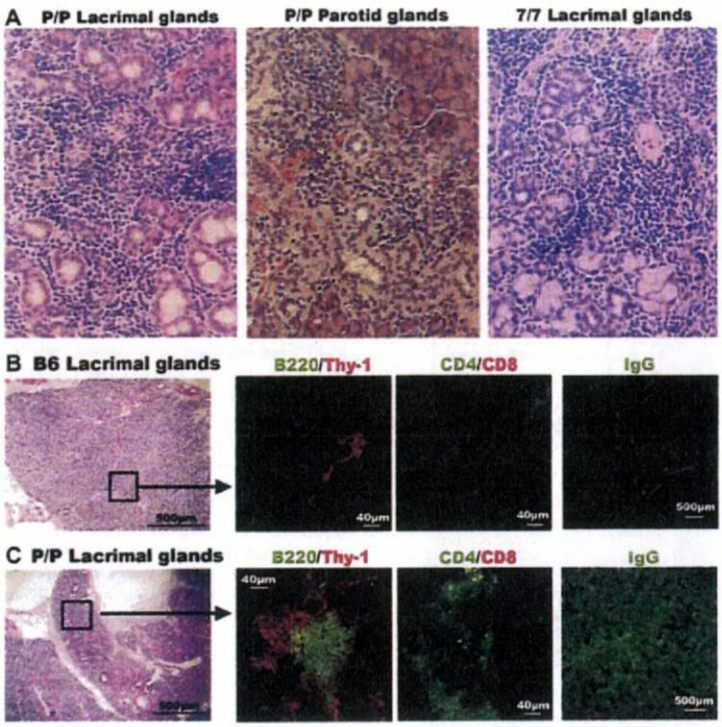

Figure 6. CCR7- or CCR7L-Deficient Mice Exhibit Autoimmune Exocrinopathy

(A) Representative sections of indicated exocrine glands from CCR7L-deficient *plt/plt* mice (P/P) and CCR7-deficient mice (7/7) show that acinar cells in the lacrimal and parotid glands are definitively destoyed in the mutant mice, presenting clear evidence of tissue damage in the mutant mice.

(B and C) Serial sections of lacrimal glands from B6 mice (B) and CCR7L-deficient *plt/plt* mice (P/P) (C) were stained with hematoxylin and eosin or with indicated antibodies. Antibodies used were specific for B220 (green), Thy-1 (red), CD4 (green), CD8 (red), and IgG (green). Shown are representative results of four independent analyses.

thymus are predominantly confined within the medulla even in CCR7- or CCR7L-deficient mice, it is possible that the thymocytes generated in CCR7- or CCR7L-deficient mice are unable to establish self-tolerance to a spectrum of organ-specific antigens because the developing thymocytes fail to interact with AIRE$^+$ mTEC localized in the medulla.

It is interesting to note that similar to CCR7- or CCR7L-deficient mice, AIRE-deficient mice as well as AIRE-deficient APECED patients manifest autoimmune dacryoadenitis and sialadenitis (Anderson et al., 2002; Liston et al., 2003; Kuroda et al., 2005), suggesting that a similar mechanism for the breakdown of central tolerance may be involved in the autoimmunity in these cases. The autoimmune phenotype in CCR7- or CCR7L-deficient mice is mild and restricted to lacrimal and salivary glands. It has been reported that the autoimmune phenotype in AIRE-deficient mice of C57BL/6 background is also mild, being largely limited to lacrimal and salivary glands (Jiang et al., 2005; Kuroda et al., 2005). Thus, the autoimmune phenotype in CCR7- or CCR7L-deficient mice and in AIRE-deficient mice is similarly mild and similarly restricted to lacrimal and salivary glands, at least in the C57BL/6 background. Whether or not the autoimmune phenotype in CCR7- or CCR7L-deficient mice of other genetic backgrounds, particularly the autoimmune-prone NOD background, may be broader and more severe, similar to the phenotype of AIRE-deficient mice, is still unclear and will be addressed in a separate study.

Nonetheless, AIRE-deficient mice of different genetic backgrounds as well as many APECED patients manifest autoimmunity with a spectrum that appears much wider than dacryoadenitis and sialadenitis in CCR7- or CCR7L-deficient mice of the C57BL/6 background (Nagamine et al., 1997; Aaltonen et al., 1997; Anderson et al., 2002; Jiang et al., 2005). It was recently shown that central tolerance to organ-specific antigens is induced not only directly by mTEC antigen presentation but also indirectly by bone-marrow-derived antigen-presenting cells such as DCs (Gallegos and Bevan, 2004). Our results show that DCs in the thymus of CCR7- or CCR7L-deficient mice are normally distributed in the cortex as well as in the medulla (Figure 4). Thus, the more restricted autoimmunity in CCR7- or CCR7L-deficient mice may be due at least in part to central tolerance to DC-mediated crosspresentation of a fraction of AIRE-dependent, organ-specific antigens expressed by mTEC. The milder autoimmunity in CCR7- or CCR7L-deficient mice than in AIRE-deficient mice may also be affected by the compromised immune responses in CCR7- or CCR7L-deficient mice, which are caused by the delayed lymphocyte homing to secondary lymphoid organs (Forster et al., 1999), even though our results show that the similarly mild autoimmune exocrinopathy is caused even in RAG2-deficient mice reconstituted with *plt/plt* thymocytes (Figure 7) in which CCR7/CCR7L signaling in peripheral mature T cells would exhibit no or little aberrancy. How the autoimmunity in CCR7-, CCR7L-, or AIRE-deficient mice is limited to dacryoadenitis and sialadenitis in the C57BL/6 background is still unclear.

We think it is possible that the clonal deletion of self-reactive thymocytes that are specific for a spectrum of organ-specific antigens may be affected in CCR7- or CCR7L-deficient mice, because the thymocytes from these mutant mice exhibit a significantly higher autologous mixed lymphocyte reaction than those from

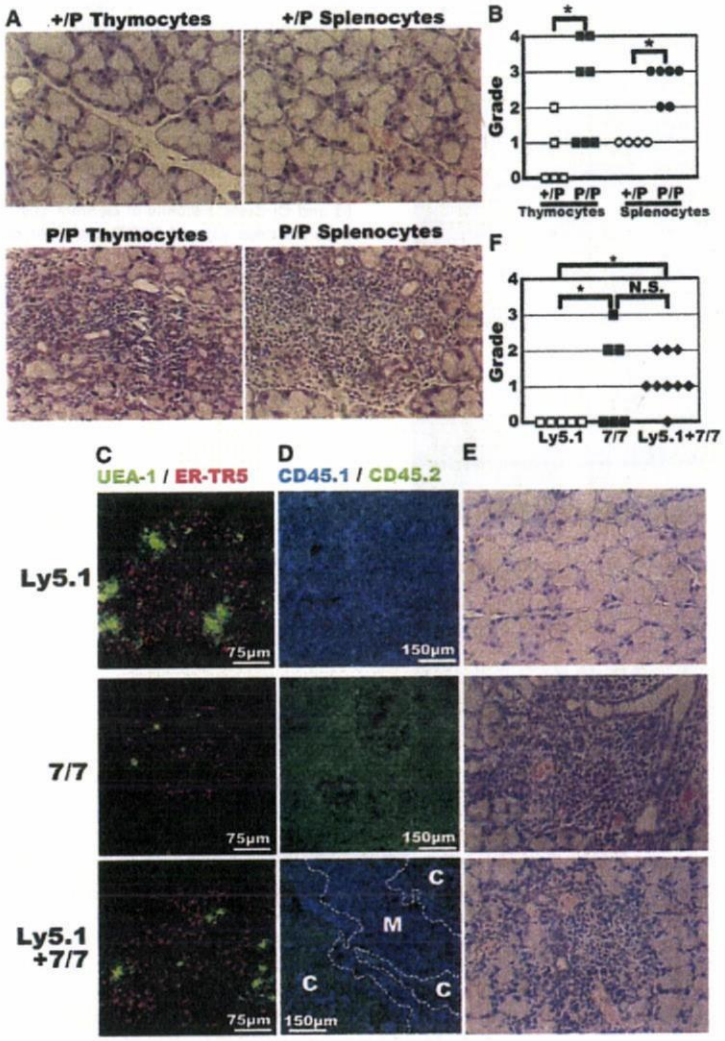

Figure 7. Exocrinopathy Is Associated with Defective Medulla Accumulation of Thymocytes

(A and B) Thymocytes generated in CCR7L-deficient mice are potent in inducing dacryoadenitis and sialadenitis. Thymocytes and splenocytes from CCR7L-deficient *plt/plt* mice (P/P) or control *+/plt* mice were transferred into nonirradiated RAG2-deficient mice. Histopathological analysis was carried out 6 weeks after the cell transfer. Tissue sections of lacrimal glands were stained with hematoxylin and eosin (A), and histological grading was performed as described in the Experimental Procedures (B).

(C–F) T cell-depleted bone marrow cells from B6.SJL-Pt_{prc} mice (Ly5.1; $CD45.1^+CD45.2^-$) and/or CCR7-deficient mice (7/7; $CD45.1^-CD45.2^+$) were transferred into nonirradiated RAG2-deficient mice. Where indicated, equal numbers of T cell-depleted bone marrow cells from B6.SJL-Pt_{prc} mice and CCR7-deficient mice were transferred (Ly5.1+7.7). Histological and flow cytometry analyses were carried out 6–8 weeks after the cell transfer. The thymuses were analyzed with multicolor confocal microscopy (C) and flow cytometry (data not shown). The UEA-1 and ER-TR5 two-color staining profiles indicate that clusters of $UEA\text{-}1^+$ cells in the medulla are generated in the B6.SJL-Pt_{prc} bone marrow chimeras (Ly5.1) and the mixed bone marrow chimeras (Ly5.1+7/7) but are defective in the CCR7-deficient bone marrow chimeras (7/7) (C). Flow cytometry analysis indicated that every mouse used for the analysis exhibited successful thymocyte reconstitution ($2.0–2.5 \times 10^8$ cells per mouse) and that the ratio of $CD45.1^+CD45.2^-$ thymocytes to $CD45.1^-CD45.2^+$ thymocytes in the mixed bone marrow chimeras was in the range of 40:60 to 60:40 (data not shown). The CD45.2 and CD45.1 two-color confocal analysis of the thymus sections (D) along with the staining of the adjacent sections with mTEC-specific ER-TR5 and UEA-1 indicates that $CD45.1^-CD45.2^+$ CCR7-deficient thymocytes are arrested in the cortex (C) and are defective in accumulating in the medulla (M) of the mixed bone marrow chimeras. Tissue sections of lacrimal glands were stained with hematoxylin and eosin (E), and histological grading was performed as described in the Experimental Procedures (F). Asterisk indicates $p < 0.05$ by the Mann-Whitney test; N.S., not significant.

normal mice (H.K. and Y.T., unpublished data), because the mixed bone marrow chimeras reconstituted with bone marrow cells from CCR7-deficient mice and normal mice exhibit the autoimmune exocrinopathy (Figure 7) and because AIRE-expressing mTEC are shown to regulate the deletion of forbidden thymocyte clones (Liston et al., 2003) rather than the generation of regulatory T cells (Anderson et al., 2005). We are currently analyzing whether the clonal deletion of organ-specific-antigen-reactive thymocytes and/or the generation of regulatory T cells may be defective in the thymus of CCR7- or CCR7L-deficient mice.

We have previously reported that negative selection is normally induced in male antigen-specific thymocytes in HY-TCR-transgenic mice and in allogeneic MHC-specific thymocytes in 2C-TCR-transgenic mice even in the absence of CCR7L (Ueno et al., 2004), indicating that negative selection to systemically ubiquitous antigens is normally induced in the absence of CCR7 signals. Perhaps, negative selection to ubiquitous antigens occurs in the cortex without migration to the medulla. We have also shown that Mtv-specific deletion of $V\beta3^+$ and $V\beta5^+$ thymocytes is normally induced in CCR7L-deficient mice (Ueno et al., 2004). It has been reported that DCs in the thymus are primarily responsible for negative selection of Mtv-reactive thymocytes (Moore et al., 1994; Ferrero et al., 1997). Our results show that in CCR7- or CCR7L-deficient mice as well as in normal

mice, DCs are localized mostly in the medulla and sparsely in the cortex. Thus, it is possible that the sparsely localized DCs in the cortex may be capable of inducing negative selection of Mtv-reactive thymocytes in the absence of CCR7 signals and without the medulla migration. The average lifespan of SP thymocytes in the thymus is 12 days (Egerton et al., 1990; Scollay and Godfrey, 1995), and the developmental kinetics of the SP thymocytes is undisturbed in the absence of CCR7 signals (Figure 1); thus, 12 days in the cortex may be sufficient for developing SP thymocytes to be negatively selected with Mtv-superantigens presented by DCs.

In conclusion, the present results indicate that the CCR7-dependent accumulation of positively selected thymocytes in the medulla is not essential for the maturation or export of thymocytes, suggesting that similar to the medulla, the thymic cortex may be capable of supporting the development and export of mature thymocytes. On the other hand, the cortex-to-medulla migration of developing thymocytes is essential for establishing central tolerance, suggesting that the developing thymocytes need to directly interact with mTEC in order to establish central tolerance to some organ-specific antigens.

Experimental Procedures

Mice

CCR7-deficient mice (Forster et al., 1999) and CCR7L-deficient *plt/plt* mice (Nakano et al., 1998) were backcrossed to C57BL/6 mice for six generations. *plt/plt* mice of BALB/c background were also used. RAG2-deficient mice and B6.SJL-Pt_{prc} mice were kindly provided by Dr. F. Alt (Shinkai et al., 1993) and Dr. H. Nakauchi, respectively. C57BL/6 (B6) mice were obtained from SLC, Shizuoka, Japan. Mice were bred and maintained under specific pathogen-free conditions in our animal facility, and experiments were performed with consent from the Animal Experimentation Committee of the University of Tokushima.

BrdU Labeling

For the detection of BrdU incorporation, adult mice were injected intraperitoneally twice with 2 mg BrdU/mouse at 4 hr intervals. Thymocytes were harvested at indicated time points after the injection. Cells that incorporated BrdU were detected with an FITC BrdU Flow Kit according to the manufacturer's instructions (BD Biosciences).

FTY720 Treatment

FTY720 (Novartis Pharma) was dissolved in saline and administered into the peritoneal cavity of adult mice at the dose of 20 μg per day for 10 days. Mice were analyzed on the day after the last administration.

Cell Transfer into RAG2-Deficient Mice

Thymocytes, splenocytes, or T cell-depleted bone marrow cells from female mice (3×10^7) were injected intravenously into nonirradiated RAG2-deficient female mice. Mice were analyzed 6–8 weeks after the cell transfer.

Multicolor Confocal Analysis

Frozen sections (5–10 μm) were fixed with acetone and stained with the following antibodies: Alexa 488-conjugated anti-CD4 (GK1.5), FITC-conjugated anti-B220 (RA3-6B2), Alexa 633-conjugated mTEC-specific ER-TR5 (van Vliet et al., 1984), and Alexa 633-conjugated anti-mouse IgG antibodies. Alexa 546-conjugated UEA-1 was also used. Biotinylated antibodies specific for CD8 (53-6-72), CD11c (HL-3), CD31 (clone 390), Thy1.2 (30-H12), and CD45.2 (clone 104) were visualized with Alexa 488-, Alexa 568-, or Alexa 633-conjugated streptavidin (Molecular Probes). The staining with anti-CD62L (MEL-14), cTEC-specific ER-TR4 (van Vliet et al., 1984), and fibroblast-specific ER-TR7 (van Vliet et al., 1984) was visualized with Alexa 488- or Alexa 633-conjugated anti-rat IgG (Molecular Probes). The staining with anti-CD45.1 antibody (clone A20) was visualized with Alexa 633-conjugated anti-mouse IgG (Molecular Probes). The images were acquired with a TCS SP2 confocal laser-scanning microscope (Leica) equipped with Ar and He-Ne lasers (excitations at 488, 568, and 633 nm) and analyzed with Leica Confocal software version 2.6.

Where indicated, frozen sections were labeled with rabbit anti-mouse pan-cytokeratin antibody (wide screen, Dako), mTEC-specific MTS-10 (Godfrey et al., 1990), and anti-AIRE antibody (clone 5H12) (Liston et al., 2004) followed by Alexa 647-conjugated anti-rabbit IgG (Molecular Probes), biotinylated anti-rat IgM (Southern Biotech), and FITC-labeled anti-rat IgG2c (Southern Biotech) antibodies. Biotinylated antibody was visualized with Alexa 568-conjugated streptavidin. The confocal images were acquired with a Bio-Rad MRC 1024 with a three-line Kr/Ag laser (excitations at 488, 568, and 647 nm) and were analyzed with Bio-Rad LaserSharp software version 3.2.

Histopathology

Paraformaldehyde-fixed tissues were embedded in paraffin. The sections (4 μm) were stained with hematoxylin and eosin. Histological grading of inflammatory lesions was carried out according to the method originally reported by White and Casarett (1974) as follows (Ishimaru et al., 2000): a score of 1 indicates that one to five foci being composed of more than 20 mononuclear cells per focus were seen; a score of 2 indicates that more than five such foci were seen but without significant parenchymal damage; a score of 3 indicates degeneration of parenchymal tissue; and a score of 4 indicates extensive infiltration of the glands with mononuclear cells and extensive parenchymal damage.

Multicolor Flow Cytometry Analysis

Single-cell suspensions were stained with FITC-labeled, PE-labeled, APC-labeled, and/or biotinylated antibodies as described (Ueno et al., 2002, 2004). Biotinylated antibodies were detected with PE- or APC-conjugated streptavidin (Molecular Probes) or Cy7-APC-conjugated streptavidin (Caltag Laboratories). Labeled monoclonal antibodies and normal IgG controls were obtained from BD Biosciences and eBiosciences. Staining with CCL19-Ig (a gift from Dr. Kunio Hieshima) was visualized with biotinylated anti-human IgG and APC-conjugated streptavidin (Ueno et al., 2004). Multicolor flow cytometry analysis was performed with two-laser FACS-Calibur or FACS-Vantage (Becton Dickinson). Data were obtained with Cell Quest software for viable cells that were determined based on measurements of forward light scatter intensity and propidium iodide exclusion.

Quantitative RT-PCR Analysis

Total cellular RNA was reverse-transcribed by using SuperScript II Reverse Transcriptase (Life Technologies) and oligo-dT oligonucleotide. cDNA was polymerase chain reaction (PCR) amplified with a SYBR Green PCR Master Mix and an ABI PRISM Sequence Detection System (Applied Biosystems) for CCR7 (5′-TGTACGTCAGTA TCACCAGC-3′ and 5′-TTTTCCAGGTGTGCTTCTGC-3′), S1P1 (5′-GTGTAGACCCAGAGTCCTGCG-3′ and 5′-AGCTTTTCCTTGGCTG GAGAG-3′), and GAPDH (5′-CCGGTGCTGAGTATGTCGTG-3′ and 5′-CAGTCTTCTGGGTGGCAGTG-3′). Amplified signals were confirmed to be single bands by using gel electrophoresis and were normalized to GAPDH levels.

Acknowledgments

We thank Drs. Hamish Scott and Daniel Gray for AIRE expression analysis; Drs. Hideki Nakano and Terutaka Kakiuchi for *plt/plt* mice; Dr. Fred Alt for RAG2-knockout mice; Dr. Willem van Ewijk for ER-TR monoclonal antibodies; Dr. Kunio Hieshima for CCL19-Ig; Drs. Takeshi Nitta and Norimasa Iwanami for reading the manuscript; and Novartis Pharma for FTY720. This work was supported by Grants-in-Aid for Scientific Research from the MEXT and JSPS, the JSPS Core-to-Core Program, and the JSPS Center of Excellence Program, and the University of Tokushima pilot research program.

Received: June 23, 2005
Revised: October 31, 2005
Accepted: December 27, 2005
Published: February 14, 2006

References

Aaltonen, J., Bjorses, P., Perheentupa, J., Horelli-Kuitunen, N., Palotie, A., Peltonen, L., Lee, Y.S., Francis, F., Henning, S., Thiel, C., et al. (1997). An autoimmune disease, APECED, caused by mutations in a novel gene featuring two PHD-type zinc-finger domains. Nat. Genet. *17*, 399–403.

Akiyama, T., Maeda, S., Yamane, S., Ogino, K., Kasai, M., Kajiura, F., Matsumoto, M., and Inoue, J. (2005). Dependence of self-tolerance on TRAF6-directed development of thymic stroma. Science *308*, 248–251.

Allende, M.L., Dreier, J.L., Mandala, S., and Proia, R.L. (2004). Expression of the sphingosine 1-phosphate receptor, S1P1, on T-cells controls thymic emigration. J. Biol. Chem. *279*, 15396–15401.

Anderson, G., and Jenkinson, E.J. (2001). Lymphostromal interactions in thymic development and function. Nat. Rev. Immunol. *1*, 31–40.

Anderson, M.S., Venanzi, E.S., Klein, L., Chen, Z., Berzins, S.P., Turley, S.J., von Boehmer, H., Bronson, R., Dierich, A., Benoist, C., and Mathis, D. (2002). Projection of an immunological self shadow within the thymus by the aire protein. Science *298*, 1395–1401.

Anderson, M.S., Venanzi, E.S., Chen, Z., Berzins, S.P., Benoist, C., and Mathis, D. (2005). The cellular mechanism of Aire control of T cell tolerance. Immunity *23*, 227–239.

Benz, C., Heinzel, K., and Bleul, C.C. (2004). Homing of immature thymocytes to the subcapsular microenvironment within the thymus is not an absolute requirement for T cell development. Eur. J. Immunol. *34*, 3652–3663.

Bjorses, P., Pelto-Huikko, M., Kaukonen, J., Aaltonen, J., Peltonen, L., and Ulmanen, I. (1999). Localization of the APECED protein in distinct nuclear structures. Hum. Mol. Genet. *8*, 259–266.

Blackburn, C.C., Manley, N.R., Palmer, D.B., Boyd, R.L., Anderson, G., and Ritter, M.A. (2002). One for all and all for one: thymic epithelial stem cells and regeneration. Trends Immunol. *23*, 391–395.

Bleul, C.C., and Boehm, T. (2000). Chemokines define distinct microenvironments in the developing thymus. Eur. J. Immunol. *30*, 3371–3379.

Boehm, T., Scheu, S., Pfeffer, K., and Bleul, C.C. (2003). Thymic medullary epithelial cell differentiation, thymocyte emigration, and the control of autoimmunity require lympho-epithelial cross talk via LTβR. J. Exp. Med. *198*, 757–769.

Bousso, P., Bhakta, N.R., Lewis, R.S., and Robey, E. (2002). Dynamics of thymocyte-stromal cell interactions visualized by two-photon microscopy. Science *296*, 1876–1880.

Brinkmann, V., Davis, M.D., Heise, C.E., Albert, R., Cottens, S., Hof, R., Bruns, C., Prieschl, E., Baumruker, T., Hiestand, P., et al. (2002). The immune modulator FTY720 targets sphingosine 1-phosphate receptors. J. Biol. Chem. *277*, 21453–21457.

Burkly, L., Hession, C., Ogata, L., Reilly, C., Marconi, L.A., Olson, D., Tizard, R., Cate, R., and Lo, D. (1995). Expression of relB is required for the development of thymic medulla and dendritic cells. Nature *373*, 531–536.

Campbell, J.J., Pan, J., and Butcher, E.C. (1999). Developmental switches in chemokine responses during T cell maturation. J. Immunol. *163*, 2353–2357.

Chiba, K., Yanagawa, Y., Masubuchi, Y., Kataoka, H., Kawaguchi, T., Ohtsuki, M., and Hoshino, Y. (1998). FTY720, a novel immunosuppressant, induces sequestration of circulating mature lymphocytes by acceleration of lymphocyte homing in rats. I. FTY720 selectively decreases the number of circulating mature lymphocytes by acceleration of lymphocyte homing. J. Immunol. *160*, 5037–5044.

Egerton, M., Scollay, R., and Shortman, K. (1990). Kinetics of mature T-cell development in the thymus. Proc. Natl. Acad. Sci. USA *87*, 2579–2582.

Fairchild, P.J., and Austyn, J.M. (1990). Thymic dendritic cells: phenotype and function. Int. Rev. Immunol. *6*, 187–196.

Farr, A.G., Dooley, J.L., and Erickson, M. (2002). Organization of thymic medullary epithelial heterogeneity: implications for mechanisms of epithelial differentiation. Immunol. Rev. *189*, 20–27.

Ferrero, I., Anjuere, F., MacDonald, H.R., and Ardavin, C. (1997). In vitro negative selection of viral superantigen-reactive thymocytes by thymic dendritic cells. Blood *90*, 1943–1951.

Fink, P.J., Gallatin, W.M., Reichert, R.A., Butcher, E.C., and Weissman, I.L. (1985). Homing receptor-bearing thymocytes, an immunocompetent cortical subpopulation. Nature *313*, 233–235.

Flotte, T.J., Springer, T.A., and Thorbecke, G.J. (1983). Dendritic cell and macrophage staining by monoclonal antibodies in tissue sections and epidermal sheets. Am. J. Pathol. *111*, 112–124.

Forster, R., Schubel, A., Breitfeld, D., Kremmer, E., Renner-Muller, I., Wolf, E., and Lipp, M. (1999). CCR7 coordinates the primary immune response by establishing functional microenvironments in secondary lymphoid organs. Cell *99*, 23–33.

Gabor, M.J., Godfrey, D.I., and Scollay, R. (1997). Recent thymic emigrants are distinct from most medullary thymocytes. Eur. J. Immunol. *27*, 2010–2015.

Gallegos, A.M., and Bevan, M.J. (2004). Central tolerance to tissue-specific antigens mediated by direct and indirect antigen presentation. J. Exp. Med. *200*, 1039–1049.

Godfrey, D.I., Izon, D.J., Tucek, C.L., Wilson, T.J., and Boyd, R.L. (1990). The phenotypic heterogeneity of mouse thymic stromal cells. Immunology *70*, 66–74.

Gotter, J., and Kyewski, B. (2004). Regulating self-tolerance by deregulating gene expression. Curr. Opin. Immunol. *16*, 741–745.

Gray, D.H., Ueno, T., Chidgey, A.P., Malin, M., Goldberg, G.L., Takahama, Y., and Boyd, R.L. (2005). Controlling the thymic microenvironment. Curr. Opin. Immunol. *17*, 137–143.

Ishimaru, N., Yoneda, T., Saegusa, K., Yanagi, K., Haneji, N., Moriyama, K., Saito, I., and Hayashi, Y. (2000). Severe destructive autoimmune lesions with aging in murine Sjogren's syndrome through Fas-mediated apoptosis. Am. J. Pathol. *156*, 1557–1564.

Jiang, W., Anderson, M.S., Bronson, R., Mathis, D., and Benoist, C. (2005). Modifier loci condition autoimmunity provoked by Aire deficiency. J. Exp. Med. *202*, 805–815.

Kajiura, F., Sun, S., Nomura, T., Izumi, K., Ueno, T., Bando, Y., Kuroda, N., Han, H., Li, Y., Matsushima, A., et al. (2004). NF-κB-inducing kinase establishes self-tolerance in a thymic-stroma dependent manner. J. Immunol. *172*, 2067–2075.

Kato, S. (1997). Thymic microvascular system. Microsc. Res. Tech. *38*, 287–299.

Kim, C.H., Pelus, L.M., White, J.R., and Broxmeyer, H.E. (1998). Differential chemotactic behavior of developing T cells in response to thymic chemokines. Blood *91*, 4434–4443.

Kishimoto, H., and Sprent, J. (1997). Negative selection in the thymus includes semimature T cells. J. Exp. Med. *185*, 263–271.

Kuroda, N., Mitani, T., Takeda, N., Ishimaru, N., Arakaki, R., Hayashi, Y., Bando, Y., Izumi, K., Takahashi, T., Nomura, T., et al. (2005). Development of autoimmunity against transcriptionally unrepressed target antigen in the thymus of Aire-deficient mice. J. Immunol. *174*, 1862–1870.

Kwan, J., and Killeen, N. (2004). CCR7 directs the migration of thymocytes into the thymic medulla. J. Immunol. *172*, 3999–4007.

Lind, E.F., Prockop, S.E., Porritt, H.E., and Petrie, H.T. (2001). Mapping precursor movement through the postnatal thymus reveals specific microenvironments supporting defined stages of early lymphoid development. J. Exp. Med. *194*, 127–134.

Liston, A., Lesage, S., Wilson, J., Peltonen, L., and Goodnow, C.C. (2003). Aire regulates negative selection of organ-specific T cells. Nat. Immunol. *4*, 350–354.

Liston, A., Gray, D.H., Lesage, S., Fletcher, A.L., Wilson, J., Webster, K.E., Scott, H.S., Boyd, R.L., Peltonen, L., and Goodnow, C.C. (2004). Gene dosage—limiting role of Aire in thymic expression, clonal deletion, and organ-specific autoimmunity. J. Exp. Med. *200*, 1015–1026.

Liu, C., Ueno, T., Kuse, S., Saito, F., Nitta, T., Piali, L., Nakano, H., Kakiuchi, T., Lipp, M., Hollander, G.A., and Takahama, Y. (2005). The role of CCL21 in recruitment of T-precursor cells to fetal thymi. Blood *105*, 31–39.

Matloubian, M., Lo, C.G., Cinamon, G., Lesneski, M.J., Xu, Y., Brinkmann, V., Allende, M.L., Proia, R.L., and Cyster, J.G. (2004). Lymphocyte egress from thymus and peripheral lymphoid organs is dependent on S1P receptor 1. Nature *427*, 355–360.

Miller, J.F.A.P. (1961). Immunological function of the thymus. Lancet *2*, 748–749.

Misslitz, A., Pabst, O., Hintzen, G., Ohl, L., Kremmer, E., Petrie, H.T., and Forster, R. (2004). Thymic T cell development and progenitor localization depend on CCR7. J. Exp. Med. *200*, 481–491.

Moore, N.C., Anderson, G., McLoughlin, D.E., Owen, J.J., and Jenkinson, E.J. (1994). Differential expression of Mtv loci in MHC class II-positive thymic stromal cells. J. Immunol. *152*, 4826–4831.

Nagamine, K., Peterson, P., Scott, H.S., Kudoh, J., Minoshima, S., Heino, M., Krohn, K.J., Lalioti, M.D., Mullis, P.E., Antonarakis, S.E., et al. (1997). Positional cloning of the APECED gene. Nat. Genet. *17*, 393–398.

Nakano, H., Mori, S., Yonekawa, H., Nariuchi, H., Matsuzawa, A., and Kakiuchi, T. (1998). A novel mutant gene involved in T-lymphocyte-specific homing into peripheral lymphoid organs on mouse chromosome 4. Blood *91*, 2886–2895.

Palmer, E. (2003). Negative selection—clearing out the bad apples from the T-cell repertoire. Nat. Rev. Immunol. *3*, 383–391.

Plotkin, J., Prockop, S.E., Lepique, A., and Petrie, H.T. (2003). Critical role for CXCR4 signaling in progenitor localization and T cell differentiation in the postnatal thymus. J. Immunol. *171*, 4521–4527.

Ramsdell, F., Jenkins, M., Dinh, Q., and Fowlkes, B.J. (1991). The majority of CD4+8-thymocytes are functionally immature. J. Immunol. *147*, 1779–1785.

Reichert, R.A., Gallatin, W.M., Butcher, E.C., and Weissman, I.L. (1984). A homing receptor-bearing cortical thymocyte subset: implications for thymus cell migration and the nature of cortisone-resistant thymocytes. Cell *38*, 89–99.

Reichert, R.A., Weissman, I.L., and Butcher, E.C. (1986a). Phenotypic analysis of thymocytes that express homing receptors for peripheral lymph nodes. J. Immunol. *136*, 3521–3528.

Reichert, R.A., Jerabek, L., Gallatin, W.M., Butcher, E.C., and Weissman, I.L. (1986b). Ontogeny of lymphocyte homing receptor expression in the mouse thymus. J. Immunol. *136*, 3535–3542.

Rinderle, C., Christensen, H.M., Schweiger, S., Lehrach, H., and Yaspo, M.L. (1999). AIRE encodes a nuclear protein co-localizing with cytoskeletal filaments: altered sub-cellular distribution of mutants lacking the PHD zinc fingers. Hum. Mol. Genet. *8*, 277–290.

Ritter, M.A., and Boyd, R.L. (1993). Development in the thymus: it takes two to tango. Immunol. Today *14*, 462–469.

Scollay, R., and Godfrey, D.I. (1995). Thymic emigration: conveyor belts or lucky dips? Immunol. Today *16*, 268–274.

Sheard, M.A., Liu, C., and Takahama, Y. (2004). Developmental status of CD4–CD8$^+$ and CD4+CD8$^-$ thymocytes with medium expression of CD3. Eur. J. Immunol. *34*, 25–35.

Shinkai, Y., Koyasu, S., Nakayama, K., Murphy, K.M., Loh, D.Y., Reinherz, E.L., and Alt, F.W. (1993). Restoration of T cell development in RAG-2-deficient mice by functional TCR transgenes. Science *259*, 822–825.

Takahama, Y., Letterio, J.J., Suzuki, H., Farr, A.G., and Singer, A. (1994). Early progression of thymocytes along the CD4/CD8 developmental pathway is regulated by a subset of thymic epithelial cells expressing transforming growth factor beta. J. Exp. Med. *179*, 1495–1506.

Ueno, T., Hara, K., Willis, M.S., Malin, M.A., Hopken, U.E., Gray, D.H., Matsushima, K., Lipp, M., Springer, T.A., Boyd, R.L., et al. (2002). Role for CCR7 ligands in the emigration of newly generated T lymphocytes from the neonatal thymus. Immunity *16*, 205–218.

Ueno, T., Saito, F., Gray, D.H., Kuse, S., Hieshima, K., Nakano, H., Kakiuchi, T., Lipp, M., Boyd, R.L., and Takahama, Y. (2004). CCR7 signals are essential for cortex-to-medulla migration of developing thymocytes. J. Exp. Med. *200*, 493–505.

Ushiki, T. (1986). A scanning electron-microscopic study of the rat thymus with special reference to cell types and migration of lymphocytes into the general circulation. Cell Tissue Res. *244*, 285–298.

van Ewijk, W., Shores, E.W., and Singer, A. (1994). Crosstalk in the mouse thymus. Immunol. Today *15*, 214–217.

van Vliet, E., Melis, M., and van Ewijk, W. (1984). Immunohistology of thymic nurse cells. Cell. Immunol. *87*, 101–109.

White, S.C., and Casarett, G.W. (1974). Induction of experimental autoallergic sialadenitis. J. Immunol. *112*, 178–185.

Witt, C.M., Raychaudhuri, S., Schaefer, B., Chakraborty, A.K., and Robey, E.A. (2005). Directed migration of positively selected thymocytes visualized in real time. PLoS Biol. *3* (6), e160 DOI: 10.1371/journal.pbio.0030160.

Zuklys, S., Balciunaite, G., Agarwal, A., Fasler-Kan, E., Palmer, E., and Hollander, G.A. (2000). Normal thymic architecture and negative selection are associated with Aire expression, the gene defective in the autoimmune-polyendocrinopathy-candidiasis-ectodermal dystrophy (APECED). J. Immunol. *165*, 1976–1983.

FEBS Letters 580 (2006) 3699–3705

A novel apoptosis cascade mediated by lysosomal lactoferrin and its participation in hepatocyte apoptosis induced by D-galactosamine

Nobuhiko Katunuma[a,*], Quang Trong Le[a], Etsuko Murata[a], Atsushi Matsui[a], Eiji Majima[b], Naozumi Ishimaru[c], Yoshio Hayashi[c], Atsushi Ohashi[a]

[a] *Institute for Health Sciences, Tokushima Bunri University, 180 Nishihamabouji, Yamashiro-cho, Tokushima 770-8514, Japan*
[b] *APRO Life Science Institute, 124-4 Itayashima, Myojin, Seto-cho, Naruto City, Tokushima 771-0360, Japan*
[c] *School of Dentistry, Tokushima University, 3-18-15 Kuramoto-cho, Tokushima 770-8504, Japan*

Received 12 April 2006; revised 25 May 2006; accepted 26 May 2006

Available online 5 June 2006

Edited by Vladimir Skulachev

Abstract A new apoptosis cascade mediated by lysosomal lactoferrin was found in apoptotic liver induced by D-galactosamine. Caspase-3 and lactoferrin were increased in the apoptotic liver cytoplasm and serum transaminases were elevated. Recombinant lactoferrin stimulated procaspase-3 processing at 10^{-6}–10^{-7} M to an extent similar to that by granzyme B in vitro. Lactoferrin changed procaspase-3 structure susceptible to the processing. Synthetic peptide Y_{679}-K_{695} in lactoferrin molecule inhibited the processing of procaspase-3 by lactoferrin. Lactoferrin in lysosomes was decreased and lactoferrin released into cytoplasm was increased quantitatively in D-galactosamine induced apoptotic liver, and procaspase-3 in cytoplasm was processed to caspase-3.

Keywords: Apoptosis; Procaspase-3; Lactoferrin; Processing; Lysosome; D-Galactosamine

1. Introduction

Many apoptosis cascades have been reported, and mitochondrial factor mediated apoptosis cascades have been well established. Caspase-3 plays a central role in various apoptosis cascades as an executive enzyme [1–4]. In 1998, we found that an unknown protein extracted from lysosomes by digitonin enhanced procaspase-3 processing in liver cytoplasm [5,6]. After that, we determined that the activating factor was lactoferrin and suggested preliminary the existence of a new apoptosis cascade mediated by lysosomal lactoferrin [7]. This paper reports on the stimulation mechanisms of procaspase-3 processing by lactoferrin at the enzymological aspects in detail and the releasing mechanism of lysosomal lactoferrin into cytoplasm in D-galactosamine-induced apoptotic hepatocyte. The pathological aspects of severe liver injury induced by D-galactosamine have been well characterized by TUNEL staining and also DNA fragmentation [9–11]. We reported in a previous paper that caspase-3 in the cytoplasm of apoptosis liver induced by D-galactosamine was increased and the apoptosis was protected by epigallo-catechin gallate in green tea which inhibited caspase-3 [11].

As the next step, we studied the molecular mechanism underlying increases in the activity of activated caspase-3 in the cytoplasm in vivo and found that a new procaspase-3 activating protein was released into the cytoplasm from lysosomes in D-galactosamine induced apoptotic hepatocytes. We determined that this activating protein was a lactoferrin originally located in lysosomes. Recombinant pure lactoferrin was found to strongly stimulate procaspase-3 processing to form active caspase-3 as same extent to that by granzyme B in vitro, and the activation mechanisms were studied at the molecular level. We reported that releasing mechanism of lysosomal lactoferrin into the cytoplasm in D-galactosamine induced apoptotic rat liver in vivo.

This paper reports on (1) stimulation mechanism of procaspase-3 processing by lactoferrin in vitro; (2) the mechanism by which lysosomal lactoferrin is released into the cytoplasm after D-galactosamine administration in vivo; (3) the existence of a novel apoptosis cascade mediated by lysosomal lactoferrin.

2. Materials and methods

2.1. Chemicals used

Caspase-3, procaspase-3, lipopolysaccharide (LPS), and lactoferrin were all recombinant pure proteins purchased from Sigma Co. (USA). The 17 residue peptide Y_{679}-K_{695} (YEKYLGPQYVAGITNLK) of the lactoferrin molecule was chemically synthesized by Asahi Techno-glass (Chiba, Japan) with 95% purity. Aspartylglutamylvalinylaspartyl-7-amino-4-trifluoromethylcoumarin (DEVD-AFC) was purchased from Peptide Institute Inc., Osaka, Japan.

2.2. Assay of procaspase-3 processing activity

Caspase-3 activity derived from procaspase-3 was determined from the fluorescence of AFC released from DEVD-AFC [5,11], and the enzyme activity was expressed in terms of AFC released in nmol/h/μg protein or nmol/h [5,6,11]. The DEVD-AFC cleavage reaction catalysed by caspase-3 and procaspase-3 processing reaction had the same optimum pH. The rate of fluorescent AFC production from the substrate DEVD-AFC by active caspase-3 was much faster than the rate of processing reaction of procaspase-3 at the optimum pH of 7.5. AFC production could be expressed as the rate of procaspase-3 processing, because procaspase-3 processing is the rate-determining step. Negative staining of SDS–polyacrylamide gel electrophoresis (PAGE)

*Corresponding author. Fax: +81 88 622 2503.
E-mail address: katunuma@tokushima.bunri-u.ac.jp (N. Katunuma).

Abbreviations: LPS, lipopolysaccharide; AFC, 7-amino-4-trifluoromethyl-coumarin; ML, mitochondria-lysosome; AST, aspartate aminotransferase; ALT, alanine aminotransferase; PAGE, polyacrylamide gel electrophoresis; LRF, lactoferrin releasing factor

0014-5793/$32.00
doi:10.1016/j.febslet.2006.05.057

for the activator sample was performed basically according to the method of Fernandez et al. [12]. The processing activities were assayed in the 78-kDa band eluents after removing SDS with renaturing buffer.

2.3. Detection of procaspase-3 activating protein using fluorescent reverse zymography

Our new double layer fluorescent reverse zymographic method was used for the detection of procaspase-3 activating proteins [21]. The activator sample was applied to a 15% polyacrylamide gel copolymerized with DEVD-AFC as the caspase-3 substrate, and the electrophoresis was performed at 13 mA for 120 min. After removing SDS from the gel with the renaturing buffer (2.5% Triton X-100), the gel was incubated with 100 μM procaspase-3 solution at 37 °C for 30 min. The fluorescent AFC band formed by caspase-3 was detected using a UV-transilluminator [13].

2.4. Determination of amino acid sequence of the activating protein of 78-kDa

The intramolecular sequences of the activating protein isolated from the Zn-negative staining SDS–PAGE was determined using an HP G1005A protein sequencing system according to the Majima's method [14]. The protein in the 78-kDa band was digested with lysyl-endopeptidase and the peptide fragments were separated with reverse-phase HPLC on a TSK gel ODS-120 T column (Tosoh) with a linear gradient of acetonitrile in 0.05% trifluoroacetic acid. The amino acid sequences of the main separated peptides were also determined using Majima's method [14].

2.5. Confocal immunohistochemical analysis of lactoferrin located in liver lysosomes

Confocal immunofluorescence analysis was performed on liver sections from C57BL/6 mice using FITC-labeled anti-lactoferrin pAb (Cappel, Turnhout, Belgium) and PE-labeled anti-Lamp-1 mAb (Santa Cruz Biotechnology Inc., Santa Cruz, CA).

2.6. Method of administration of D-galactosamine with LPS in vivo

Rat liver apoptosis was induced by D-galactosamine treatment using Muntane's method [8] by the intraperitoneal injection of D-galactosamine 0.5 g/kg or D-galactosamine 0.5 g/kg plus LPS 50 μg/kg. Twelve hours after the injection, the rats were sacrificed to prepare the livers.

2.7. Preparation of lysosomes and cytoplasmic fraction of rat liver

The rat liver was gently homogenized with a Teflon pestle in 0.25 M cold isotonic sucrose buffer. The suspension was centrifuged at 3500 × *g* for 10 min at 4 °C to remove the nucleuses and cells. The supernatant was centrifuged at 25000 × *g* for 20 min at 4 °C to prepare the lysosome-mitochondrial (ML) fraction, and then to prepare the cytoplasm fraction, the supernatant was further centrifuged at 100000 × *g* for 60 min to remove the microsomes. To prepare pure lysosomes, a two-phase partition centrifugation method in the presence of 1 mM $CaCl_2$ was used [15]. The lysosomal fractions for the assay of procaspase-3 activation were extracted using a 40 μM digitonin solution with isotonic sucrose buffer.

2.8. Sample preparation for activity assay of the lysosomal procaspase-3 activating protein

The ML fractions of rat liver were extracted with 5 mL of digitonin solution. After concentration to 1 mL, 30 μL portion of the extract was applied to SDS gel to make SDS–PAGE. After removing the SDS, the 78-kDa fractions were eluted from the gel for determination of procaspase-3 activating activity or assay of the lactoferrin protein by the antibody. The activating activities were expressed as the AFC released nM/h/mg protein (cytoplasmic protein, lysosomal protein or SDS–PAGE band protein).

2.9. Statistical analysis

Values for expression are shown as means ± S.D. Quantitative differences between values were statistically analyzed by Dunnett's multiple comparison *t* test *P* values <0.01 were considered to be significant.

3. Results and discussion

3.1. Detection of procaspase-3 activating protein in the cytoplasm of D-galactosamine treated apoptotic liver cells

When D-galactosamine was administered intraperitoneally to rats, caspase-3 activity in the liver cytoplasm was elevated in a dose-dependent manner 12 h after injection and cotreatment with LPS enhanced the apoptosis dramatically, as shown in Table 1. The liver injury markers, aspartate aminotransferase (AST) and alanine aminotransferase (ALT), were strongly elevated in the serum. Therefore, the increases of caspase-3 may participate in D-galactosamine induced liver injury [11].

In order to elucidate the mechanism of caspase-3 elevation during the apoptosis, the activation factor of procaspase-3 in the treated liver cytoplasm was determined by the following procedure. Same amounts of cytoplasmic fraction and lyso-

Table 1
Elevation of caspase-3 in liver cytoplasm and translocation of lysosomal lactoferrin from lysosomes into cytoplasm in rat liver induced apoptosis by D-galactosamine

Treatments	Enzymes					
	In liver cytoplasm		In liver lysosomes		In serum	
	Caspase-3 (AFC nM/mg/hr)	Activator, 78 kDa (AFC nM/mg/h)	Activator, 78 kDa (AFC nM/mg/h)	Activator, 35 kDa (AFC nM/mg/h)	AST (IU/l)	ALT (IU/l)
Normal	76.50 ± 9.42	25.0 ± 18.6	612.6 ± 210	100.0	23.37 ± 3.69	4.15 ± 1.17
D-GalN (300 mg/kg)		180 ± 90.0	250.0 ± 150	95.0		
D-GalN (500 mg/kg)	1000.0 ± 360	322 ± 126.0	152.4 ± 60	110.0	247.37 ± 194.07	70.17 ± 51.15
D-GalN (700 mg/kg)		609 ± 40	20.0 ± 15	105.0		
LPS(50 μg/kg)	97.56 ± 21.65				23.33 ± 6.25	6.67 ± 1.25
D-GalN(500 mg) + LPS(50 μg/kg)	5159.73 ± 1250.37	1488.6 ± 576.9	≒0		2154.31 ± 598.02	525.94 ± 140.74

0.5 g/kg of the D-galactosamine plus 50 mg/kg of LPS was intraperitoneally injected to rats, and the 12 h after the injection, the rats were sacrificed. The procaspase-3 activating activities (lactoferrin) translocated from the lysosomes into the cytoplasm in the apoptotic hepatocyte were assayed using the method as follows. The quantitative amounts of the digitonin extracts of the lysosomes or the cytoplasm preparations were applied to make SDS–PAGE, and the procaspase-3 activating activities in the 78-kDa fractions and those in the 35-kDa fractions from the lysosomes, and also those from the cytoplasms were assayed at the same time. Furthermore, these activating protein amounts in the cytoplasm corresponded to the released lactoferrin protein amounts using ant lactoferrin antibody [18]. The activating activities were expressed as the AFC released nM/h/mg protein in the extracts of cytoplasmic protein or lysosomal protein. The reciprocal movements of the lactoferrin (procaspase-3 processing activities) in the lysosomes and the cytoplasm were observed in D-galactosamine dose-dependently. Data are shown as the means ± S.D.: $n = 3$–5, $^{*}P < 0.01$.

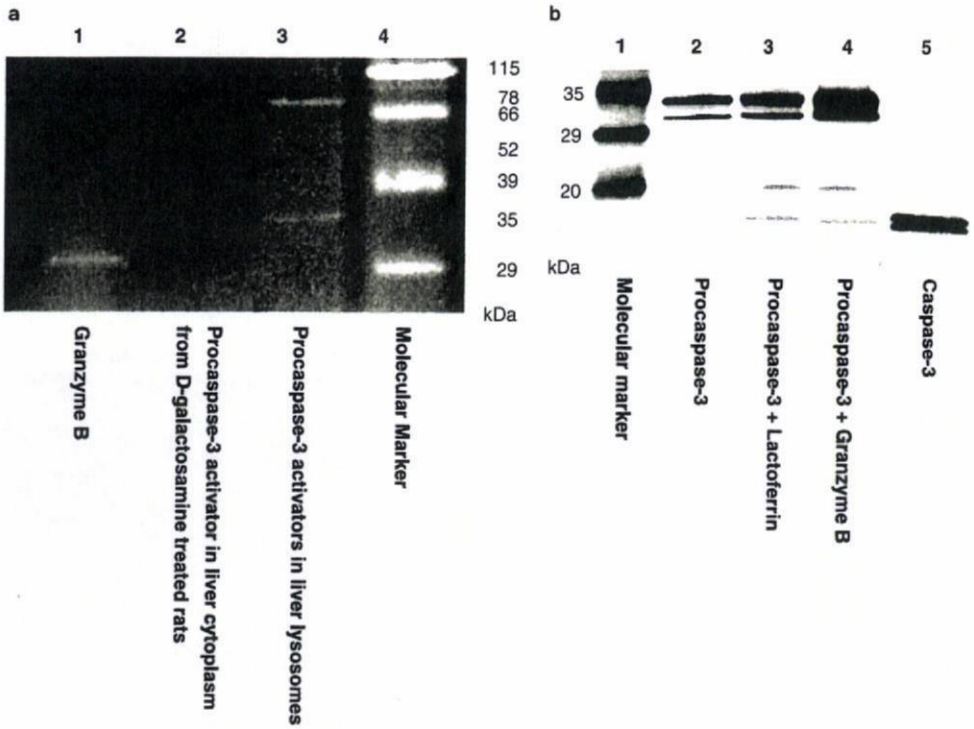

Fig. 1. (a) Detection of procaspase-3 activating proteins in rat liver treated with D-galactosamine using double-layer fluorescent reverse zymography The procaspase-3 activating proteins were detected using Katunuma's double-layer fluorescent reverse zymography; the method is described in the text [13,21]. DEVD-AFC was used as a caspase-3 substrate. Lane 1: location of granzyme B as the procaspase-3 activating enzyme in the 32-kDa band. Lane 2: Procaspase-3 activating protein in the 78-kDa band was detected in the liver cytoplasm fraction of D-galactosamine treated rats. Lane 3: Procaspase-3 activating proteins in the digitonin extracts of liver lysosome from normal rats in the 78-kDa band which corresponds to the band of lactoferrin and the 35-kDa protein band which is unknown activating protein. (b) Procaspase-3 processing products by lactoferrin. SDS–PAGE gel was stained by Coomassie blue. The products of procaspase-3 processing mediated by lactoferrin were the same as those produced by granzyme B.

somal extract of liver were applied separately to SDS gels and electrophoresis was performed. After removing the SDS from the PAGE with renaturing buffer, the procaspase-3 processing activities in the eluents were detected in the 78-kDa fraction and the 35-kDa fraction using caspase-3 formation from recombinant procaspase-3. The procaspase-3 activating protein in the 78-kDa fraction was increased in the cytoplasm and the activity in the lysosomes was decreased in a reciprocal manner, as shown in Table 1. Sufficient amounts of procaspase-3 were present in the normal cytoplasm, but active caspase-3 was not detected in the normal cytoplasm. These data suggest that the procaspase-3 activating protein is originally located in the lysosomes under normal conditions and that only the 78-kDa activating protein was released into the cytoplasm by D-galactosamine administration.

We then purified the 78-kDa activating protein from the liver lysosomes to allow identification. The partially purified activating protein from the digitonin extracts of liver lysosomes was applied to SDS gels to separate the proteins. Two kinds of activating proteins with molecular weights of 78-kDa and 35-kDa were detected using fluorescent reverse zymography for processing protease detection [13,21], as shown in Fig. 1(a) in lane 3. The 78-kDa band corresponds to recombinant lactoferrin, and the 35-kDa band is an unknown activating protein. The 35-kDa factor was not detected in the cytoplasm of the apoptotic liver, therefore, the 35-kDa factor does not participate in the apoptosis.

3.2. *Purification and identification of the 78-kDa lysosomal activating protein as lactoferrin*

A procaspase-3 activating protein was extracted with a 40 μM digitonin isotonic sucrose buffer from the purified lysosomes of bovine liver. The specific activity of the procaspase-3 processing enzyme in the digitonin extracts was 2.5 nmol AFC/h/μg protein (formed from DEVD-AFC). The extracted protein was fractionated with 40–60% ammonium sulfate and then heat treated at 70 °C for 1 min. The supernatant was further fractionated with 40–50% ethanol at −20 °C. The fraction was subsequently subjected to column chromatography using Superdex G75, Mono Q and then Hydroxyapatite CHT5-I BIO-RAD. The specific activity of the final active fraction was about 100 nmol AFC/h/μg protein. The purity was increased about 40 times compared with that of the digitonin extracts. The purified sample had about the same activating activity as that of the recombinant pure lactoferrin. The purified fraction showed almost a single protein on the SDS–PAGE.

The intramolecular amino acid sequence of the purified 78-kDa activating protein eluted from the negative zinc staining band in the SDS–PAGE was determined [12]. The sample was hydrolyzed with lysyl-endopeptidase and the peptides produced were separated using reversed-phase HPLC. The amino acid sequences of the two different parts of the separated peptides were determined. The amino acid sequences of these two peptides were completely identical with those of the corresponding parts of recombinant bovine lactoferrin. The amino

acid sequences of these two domains from the purified sample were H_{435}-P_{444} (n-H-S-S-L-D-C-V-L-R-P-c) and N_{653}-E_{661} (n-N-L-L-F-N-D-N-T-E-c). The molecular weight (78-kDa) and the isoelectric point (5.4–5.7) of the purified activating protein were the same as those of the recombinant bovine lactoferrin. The processing product of procaspase-3 by the 78-kDa protein was the same as that by recombinant lactoferrin as demonstrated in Fig. 1(b). The same processing products of procaspase-3 by granzyme B were demonstrated.

3.3. Subcellular localization of lactoferrin in liver lysosomes

A two-phase Ficoll partition centrifugation method in 1 mM $CaCl_2$ was used to determine the subcellular localization of the activating protein in rat liver [15]. The activating activity was detected only in the lysosomal fraction, coinciding with the location of cathepsin L, while the activity was not detected in the swollen mitochondrial fraction, coinciding with glutamic dehydrogenase (data not shown). The confocal immunohistochemical staining of mouse liver, using a monoclonal anti-lactoferrin antibody and a PF-labeled anti-Lamp-1 antibody as lysosomal markers, was used to determine the subcellular localization of the lactoferrin (see Section 2). The lactoferrin was detected only in the lysosomal particles located in the cell membrane area, as Fig. 2 shows.

3.4. Activation mechanism of procaspase-3 by lactoferrin

The activation mode of the procaspase-3 processing reaction mediated by pure lactoferrin was analyzed. Procaspase-3 was originally processed slowly via autocatalytic reaction in Tris–HCl buffer at pH 7.5 and 37 °C in vitro, and 1×10^{-7} M lactoferrin strongly accelerated the autocatalytic processing to several-fold, as shown in Fig. 3(a). The procaspase-3 processing rate mediated by 1×10^{-6} M lactoferrin was about 7000–8000 nM AFC formed per hour, while the autocatalytic rate was about 1000–1600 nM AFC formed per hour. Specific activity of procaspase-3 processing reaction catalyzed by lactoferrin was 432 nM AFC formed/h/mg protein, while that by granzyme B was 515 nM AFC formed/h/mg. Both catalytic activities showed about the same level. The lactoferrin mediated procaspase-3 activating reaction was not inhibited by various cysteine protease inhibitors, including E-64 or serine protease inhibitors, and anti-granzyme B antibody also did not inhibit the activation reaction (data abbreviated). Since both apo-lactoferrin and holo-lactoferrin had the same activation function and 1×10^{-7} M lactoferrin showed the enough activation (Fig. 3(b)), the iron atom itself and the domains of the iron atom binding did not participate in this activation reaction. The processing products of recombinant procaspase-3 mediated by lactoferrin were the same as those mediated by granzyme B by Western blotting using the anti-caspase-3 antibody as shown in Fig. 1(b).

With regard to the activating mechanism of procaspase-3 processing by the lactoferrin, a lactoferrin–procaspase-3 complex may be formed as an intermediate step. The lactoferrin may play a chaperone-like role to alter the tertiary structure of the procaspase-3 and render it more susceptible to being processed. The binding affinity for making the complex was shown in Fig. 3(c), and the K_m is about 1×10^{-11} M. The lactoferrin did not have any effect on the caspase-3 assay reaction. The domain which participates in the binding of procaspase-3

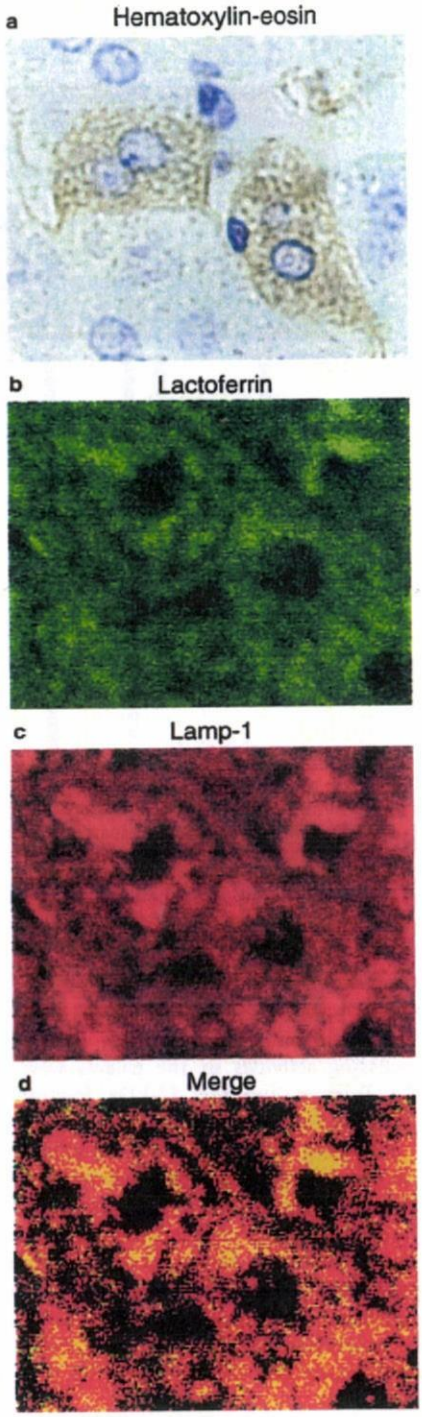

Fig. 2. Subcellular localization of lactoferrin in rat liver using confoc immunohistochemical staining. (a) Hematoxylin-eosin staining hepatocytes. (b) Lactoferrin localization in lysosomes using an ant lactoferrin antibody in green. (c) Lysosome staining by PF-labele anti-Lamp-1 antibody in red. (d) Merged profile of lactoferrin an lysosomal marker Lamp-1. The lactoferrin was stained in th lysosomes located in the cell membrane area.

to the lactoferrin molecule was estimated to be Y_{679}-K_{695} (YI KYLGPQYVAGITNLK) in lactoferrin. We reported prev ously that this domain was an inhibitory site of th

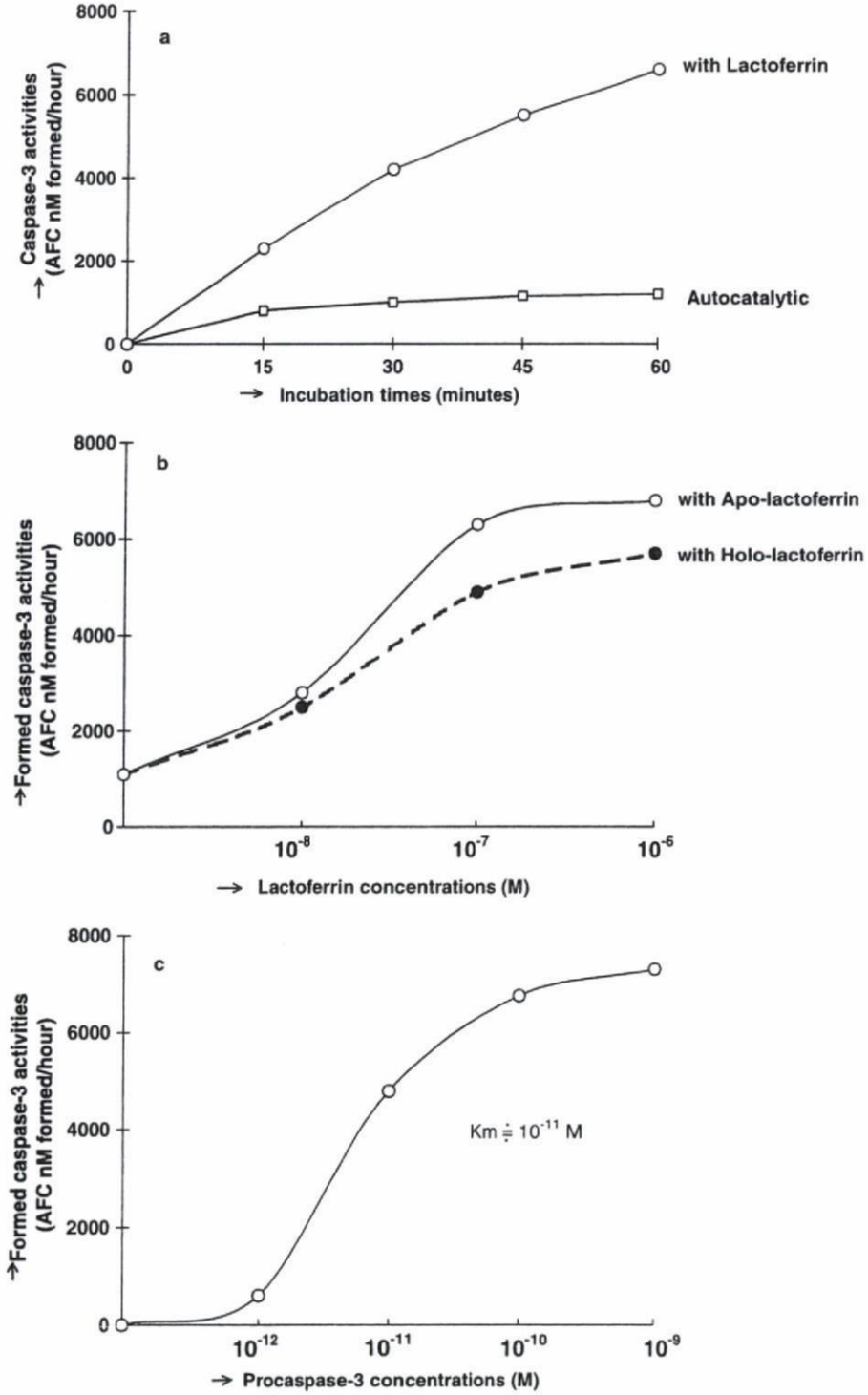

Fig. 3. Activating mechanisms of procaspase-3 processing reaction mediated by lactoferrin. The procaspase-3 processing activity was assayed by the formed caspase-3 activity and the formed caspase-3 activities from procaspase-3 are expressed as AFC formed nM/h in the vertical axis. Panel (a): Reaction time course of procaspase-3 processing with lactoferrin. Panel (b): Dose-dependent activations of the procaspase-3 processing reaction mediated by holo-lactoferrin or apo-lactoferrin. Apo-lactoferrin was prepared from holo-lactoferrin by the treatments at pH 2.0. The iron atoms were released into the supernatant and no iron atoms were detected in the precipitated lactoferrin. Panel (c): Kinetical studies of the affinity of procaspase-3 for lactoferrin and the K_m value.

lactoferrin for cysteine proteases [16]. This domain is highly homologous with a common active site of the cystatin family. The synthetic peptide Y_{679}-K_{695} strongly inhibited not only the activation reaction of the processing mediated by lactoferrin, but also the autocatalytic processing reaction, as shown in Fig. 4. This peptide may disturb the binding of procaspase-3

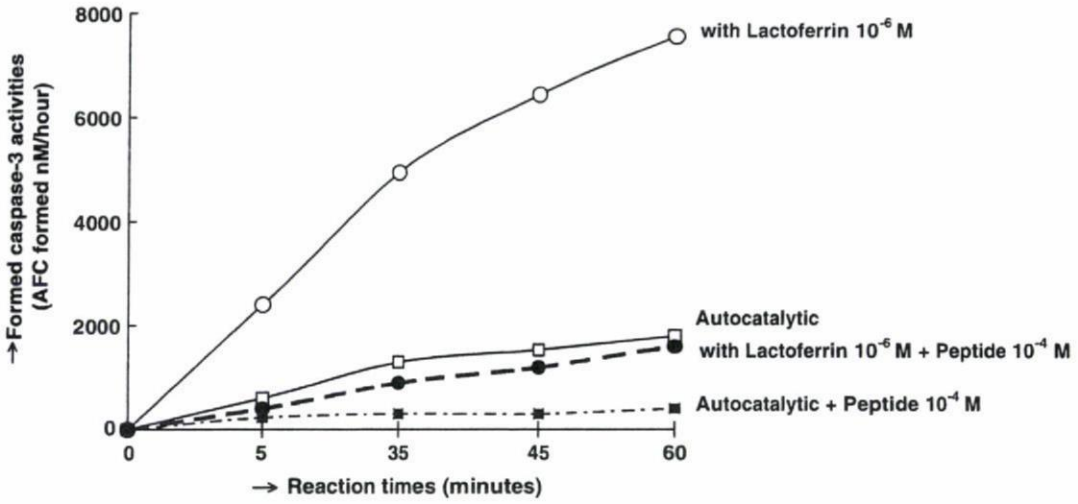

Fig. 4. Inhibition profiles of procaspase-3 processing reaction mediated by lactoferrin by synthetic peptide, Y_{679}-K_{695}, in the domain of lactoferrin molecule. Lactoferrin concentration of 1×10^{-6} M as an activator and synthetic peptide concentration of 1×10^{-4} M as the inhibitor were used. The procaspase-3 processing reaction mediated by 1×10^{-6} M lactoferrin (○–○) and inhibited by 1×10^{-4} M of the peptide (●···●) are shown in this panel. Autocatalytic processing (□–□) and inhibition with 1×10^{-4} M peptide (■···■) are also shown.

to lactoferrin. Therefore, the domain Y_{679}-K_{695} of the lactoferrin may play an important role in the acceleration function by participating in the binding of procaspase-3 to lactoferrin. To explain the practical allosteric structural changes, the X-ray co-crystallographic analysis of these complexes is required. We previously reported a similar type of chaperone-like functioning protein, a chondroitin-sulfate proteoglycan, which is a potent enhancer of the autoprocessing of procathepsin L to form the active mature cathepsin L [17]. We propose that these kinds of specific accelerator proteins, or "enzymoids", may participate in various post-translational processing reactions in general.

3.5. A new apoptosis cascade mediated by lysosomal lactoferrin

To confirm the translocation of the lactoferrin, the lactoferrin released in the cytoplasm was assayed quantitatively with antibodies to lactoferrin using Sanchez's method [18]. The lactoferrin released in the cytoplasm increased to 7 μg/mL of cytoplasm upon treatment with 700 mg/kg D-galactosamine, while no lactoferrin was detected in the normal liver cytoplasm. It is possible to consider that the lactoferrin located in the lysosomes was released into the cytoplasm by D-galactosamine administration dose-dependently in vivo as shown in Table 1, although the releasing mechanisms are not known at the present. The released procaspase-3 activating activity in

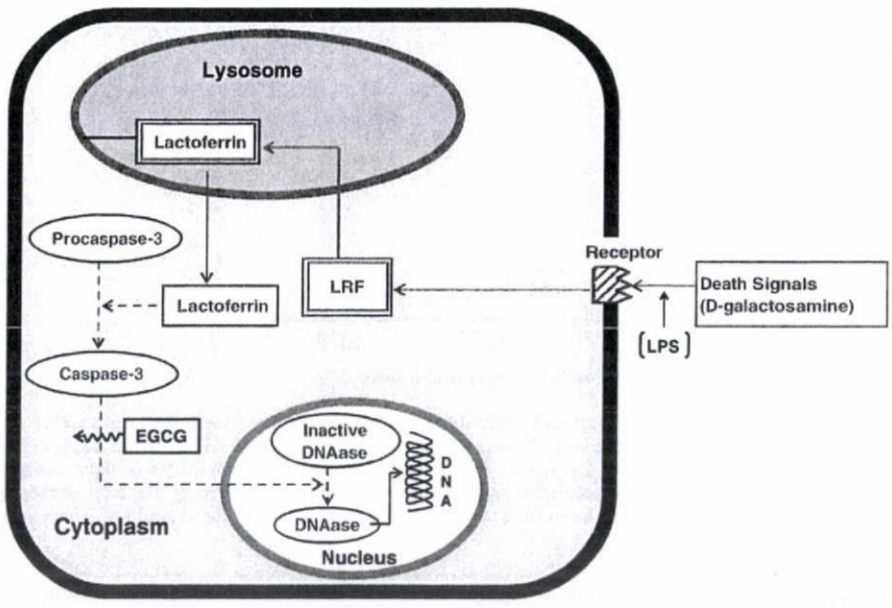

Fig. 5. Schematic illustration of a new apoptosis cascade mediated by lysosomal lactoferrin. Solid red line; the death signal transduction induced by D-galactosamine. Dotted blue line; a new apoptosis cascade mediated by lysosomal lactoferrin. LRF; unknown lactoferrin releasing factor.

the cytoplasm by D-galactosamine plus LPS treatment was 5000–6000 AFC nM/h, this activity is corresponding to the activity by 10^{-6}–10^{-7} M of lactoferrin (calculated by Fig. 3(b)). This amount (concentration) is enough to activate procaspase-3 in vitro. Sufficient amounts of procaspase-3 are located in the normal liver cytoplasm, but caspase-3 was not present in the normal cytoplasm. As a model experiment, the caspase-3 activity (DEVD-AFC cleaving activity) in a normal liver cytoplasm preparation was found to be strongly enhanced by the addition of recombinant lactoferrin in vitro. We reported in our previous papers that the caspase-3 activity in the normal liver cytoplasm was enhanced by the addition of digitonin extracts of lysosomes in vitro [5,6]. The activities of other known caspases [6,8,11,13], which are the proteolytic signal transduction caspases, were not changed by the D-galactosamine treatment (data not shown). When a suitable death signal was added, the corresponding activating protein was translocated from the different organelles into the cytoplasm, resulting in increases in caspase-3 mediated apoptosis, in general [1]. The releasing mechanism of lysosomal lactoferrin by D-galactosamine treatment is not known. Quintero et al. reported that prostaglandin E1 protection against apoptosis induced by D-galactosamine is not related to the modulation of intracellular free radical production in primary culture of rat hepatocyte [19]. However, we have not any direct evidences on the releasing mechanisms of lysosomal lactoferrin into cytoplasm by D-galactosamine induced hepatocyte apoptosis. Fujita et al. reported that lactoferrin stimulated the apoptosis of azoxymethane-induced tumors and the elevation of active forms of caspases-3 and 8. But little is known about the mechanisms at the molecular level. The problem of this report is that the lactoferrin was administrated perorally with diet, it is difficult to consider that the 72-kDa lactoferrin is effectively absorbed from intestine [20]. The caspase-3 activity was dramatically elevated in the cytoplasm of D-galactosamine induced apoptotic hepatocytes and administration of epigallo-catechin gallate which was strong inhibitor for caspase-3 activity suppressed the elevation of caspase-3 activity in the cytoplasm and protected the hepatocyte apoptosis [11]. Our proposed new apoptotic cascade mediated by lysosomal lactoferrin is illustrated schematically in Fig. 5.

Acknowledgements: This work was supported by the Grants-in-aid from the Japanese Ministry of Education, Sciences and Culture. We thank Professor Guy Salvesen for his useful advice and thank Rika Takahashi for her valuable help in preparing this manuscript.

References

[1] Salvesen, G.S. and Dixit, V.M. (1997) Caspases, intracellular signaling by proteolysis. Cell 91, 443–446.
[2] Liu, X., Kim, C.N., Yang, J., Jemmerson, R. and Wang, X. (1996) Induction of apoptotic program in cell-free extracts: requirement for dATP and cytochrome *c*. Cell 86, 147–157.
[3] Kluck, R.M., Bossy-Wetzel, E., Green, D.R. and Newmeyer, D.D. (1997) The release of cytochrome *c* from mitochondria: a primary site for Bcl-2 regulation of apoptosis. Science 275, 1132–1136.
[4] Li, P., Nijhawan, D., Budihardjo, I., Srinivasula, S.M., Ahmad, M., Alnemri, E.S. and Wang, X. (1997) Cytochrome *c* and dATP-dependent formation of Apaf-1/caspase-9 complex initiates an apoptotic protease cascade. Cell 91, 479–489.
[5] Ishisaka, R., Utsumi, T., Yabuki, M., Kanno, T., Furuno, T., Inoue, M. and Utsumi, K. (1998) Activation of caspase-3 like protease by digitonin-treated lysosomes. FEBS Lett. 435, 233–236.
[6] Ishisaka, R., Utsumi, T., Kanno, T., Arita, K., Katunuma, N., Akiyama, J. and Utsumi, K. (1999) Participation of a cathepsin L-type protease in the activation of caspase-3. Cell Struct. Funct. 24, 465–470.
[7] Katunuma, N., Murata, E., Le, Q.T., Hayashi, Y. and Ohashi, A. (2004) New apoptosis cascade mediated by lysosomal enzyme and its protection by epigallo-catechin gallate. Adv. Enzyme Regul. 44, 1–10.
[8] Muntane, J., Montero, J.L., Marchal, T., Perez-Seoane, C., Lozano, J.M., Fraga, E., Pintado, C., de la Mata, O. and Mino, G. (1998) Effect of PGE_1 on TNF-α status and hepatic D-galactosamine-induced apoptosis in rats. J. Gastroent. Hepatol. 13, 197–207.
[9] Galanos, C., Freudenberg, M.A. and Reutter, W. (1979) Galactosamine-induced sensitization to the lethal effects of endotoxin. Proc. Natl. Acad. Sci. USA 76, 5939–5943.
[10] Thornberry, N.A., Bull, H.G., Calaycay, J.R., Chapman, K.T., Howard, A.D., Kostura, M.J., Kostura, M.J., Miller, D.K., Molineaux, S.M., Weidner, J.R., Aunins, J., Elliston, K.O., Ayala, Jm., Casano, F.J., Chin, J., Ding, G.J.-F., Egger, L.A., Gaffney, E.P., Limjuco, G., Palyha, O.C., Raju, S.M., Ralond, A.M., Salley, J.P., Yamin, T.T., Lee, T.D., Shively, J.E., MacCross, M., Mumford, R.A., Schumidt, J.A. and Tocci, M.J. (1992) A novel heterodimeric cysteine protease is required for interleukin-1 beta processing in monocytes. Nature 356, 768–774.
[11] Katunuma, N., Ohashi, A., Sano, E., Ishimaru, N., Hayashi, Y. and Murata, E. (2006) Catechin derivatives: specific inhibitor for caspases-3, 7 and 2, and the prevention of apoptosis at the cell and animal levels. FEBS Lett. 580, 741–746.
[12] Fernandez-Patron, C., Castellanos-Serra, L. and Rodriguez, P. (1992) Reverse staining of sodium dodecyl sulfate polyacrylamide gels by imidazole-zinc salts: sensitive detection of unmodified proteins. Biotechniques 12, 564–573.
[13] Le, Q.T., Ohashi, A., Hirose, S. and Katunuma, N. (2005) Reverse zymography using fluorogenic substrates for protease inhibitor detection. Electrophoresis 26, 1038–1045.
[14] Majima, E., Ishida, M., Miki, S., Shinohara, Y. and Terada, H. (2001) Specific labeling of the bovine heart mitochondrial phosphate carrier with fluorescein 5-isothiocyanate: roles of Lys185 and putative adenine nucleotide recognition site in phosphate transport. J. Biol. Chem. 276, 9792–9799.
[15] Osada, J., Aylagas, H., Sanchez-Prieto, J., Sanchez-Vegazo, I. and Palacios-Alaiz, E. (1990) Isolation of rat liver lysosomes by a single two-phase partition on dextran/polyethylene glycol. Anal. Biochem. 185, 249–253.
[16] Ohashi, A., Murata, E., Yamamoto, K., Majima, E., Sano, E., Le, Q.T. and Katunuma, N. (2003) New functions of lactoferrin and β-casein in mammalian milk as cysteine protease inhibitors. BBRC 306, 98–103.
[17] Kihara, M., Kakegawa, H., Matano, Y., Murata, E., Tsuge, H., Kido, H. and Katunuma, N. (2002) Chondroitin sulfate proteoglycan is a potent enhancer in the processing of procathepsin L. Biol. Chem. 383, 1925–1929.
[18] Sanchez, L., Aranda, P., Perez, M.D. and Calvo, M. (1988) Concentration of lactoferrin and transferrin throughout lactation in cow's colostrum and milk. Biol. Chem. Hoppe Seyler 369, 1005–1008.
[19] Quintero, A., Pedraza, C.A., Siendones, E., Kamal ElSaid, A.M., Colell, A., Garcia-Ruiz, C., Montero, J.L., De la Mata, M., Fernandez-Checa, J.C., Mino, G. and Muntane, J. (2002) PGE_1 protection against apoptosis induced by D-galactosamine is not related to the modulation of intracellular free radical production in primary culture of rat hepatocytes. Free Radic. Res. 36, 345–355.
[20] Fujita, K., Matsuda, E., Sekine, K., Iigo, M. and Tsuda, H. (2004) Lactoferrin enhances Fas expression and apoptosis in the colon mucosa of azoxymethane-treated rats. Carcinogenesis 25, 1961–1966.
[21] Katunuma, N., Le, Q.T., Miyauchi, R. and Hirose, S. (2005) Double-layer fluorescent zymography for processing protease detection. Anal. Biochem. 347, 208–212.

FEBS Letters 580 (2006) 741–746

Catechin derivatives: Specific inhibitor for caspases-3, 7 and 2, and the prevention of apoptosis at the cell and animal levels

Nobuhiko Katunuma[a,*], Atsushi Ohashi[a], Etsuko Sano[a], Naozumi Ishimaru[b], Yoshio Hayashi[b], Etsuko Murata[a]

[a] *Tokushima Bunri University, Institute for Health Sciences, 180 Nishihamabouji, Yamashiro-cho, Tokushima 770-8514, Japan*
[b] *The University of Tokushima Graduate School, Department of Oral Molecular Pathology, Institute of Health Biosciences, 3-18-15 Kuramoto-cho, Tokushima 770-8504, Japan*

Received 6 October 2005; revised 22 December 2005; accepted 28 December 2005

Available online 6 January 2006

Edited by Vladimir Skulachev

Abstract Tea-catechin derivatives are shown to inhibit activities of caspases-3, 2 and 7 in vitro, and prevented experimental apoptosis at the cell and animal levels. Epigallo-catechin-gallate showed the strongest inhibition at 1×10^{-7} M to these caspases, but cysteine cathepsins and caspase-8 were not inhibited. Caspase-3 inhibition showed a 2nd-order allosteric-type, but the inhibition of caspases-2 and 7 showed a non-competitive-type. The apoptosis-test using cultured HeLa cells was inhibited by these catechins. In rat hepatocytes, apoptosis was induced by D-galactosamine in vivo. In this case, caspase-3 activity in the cytoplasm, the serum aminotransferases and dUTP nick formation detected by TUNNEL-staining were effects, and these elevations were suppressed by administration of catechin.

Keywords: Catechin; Caspase-3; Apoptosis; D-Galactosamine; Serum aminotransferase

1. Introduction

Various pharmacological functions of tea-catechin derivatives have been extensively studied in recent years. Their anti-oxidant effects are well established; in addition, the possibility for prevention of oncogenesis by tea-catechins from the aspect of epidemiological statistics has been advocated. However, no reasonable explanation exists for the prevention of oncogenesis at the molecular level (see Section 4). The direct effect of tea-catechins on specific caspases with respect to apoptosis has not yet been reported. The synthetic inhibitors of substrate analogues for caspases have been reported; however, natural inhibitors have not been identified. Allosteric inhibition of caspase-3 by synthetic inhibitors was reported by Hardy et al., therefore the tertiary structures of caspases are flexible (see Section 4) [11]. We have previously shown that some tea-catechin derivatives strongly inhibited caspases-3, 2 and 7, in vitro and in vivo [1,2,5–9].

The inhibition of cultured HeLa cell apoptosis test, which is reported by Wells et al., was studied [4]. Liver injury induced by D-galactosamine with lipopolysaccharide (LPS) in vivo is well characterized to induce hepatocyte apoptosis within the pathological field, assessed by TUNNEL-staining and DNA fragmentation [1–4]. The activity of caspase-3 in the liver cytoplasm was significantly elevated, and aspartate (AST) and alanine (ALT) aminotransferases in the serum were also significantly elevated in the D-galactosamine induced apoptotic liver. These increases were suppressed by epigallo-catechin-gallate (EGCG) in vivo. EGCG is the main component of green tea. The specific inhibition of activities of caspases-3, 2 and 7 by tea-catechin derivatives in vitro and the prevention of liver cell apoptosis in vivo are reported in this paper.

2. Materials and methods

2.1. Materials

Recombinant human caspases-3, 7, 8 and 2 were purchased from Bio-Vision Co. Catechin derivatives were purchased from Wako Co. Cathepsin B and L were purchased from Sigma.

2.2. Methods

2.2.1. Inhibition assays of caspases-3, 7, 2 and 8 activities by catechin derivatives. An established method for the assay of activities of caspase-3 and caspase-7 was used [9], using the recombinant pure caspases and DEVD-AFC as the substrate. Ac-IETD-MCA was used for caspase-8 and AC-VDVAD-MCA was used for caspase-2. Enzyme activity was expressed as the released AFC (or MCA) formed nM/h/mg protein.

2.2.2. Cell-free apoptosis test using cultured HeLa cell S-100. The apoptosis assay system reported by Wells et al. is composed of cultured HeLa cell cytoplasm S-100 (4 mg protein/ml), cytochrome *c* (80 μM) and Ac-DEVD-MCA (40 μM) as the substrate for formed caspase-3 [12]. Preparation of S-100 from cultured HeLa cells was followed using the method described by Wells and Nguyen [12]. Following incubation at 37 °C for 40 min, the released fluorescent MCA in the S-100 fraction was assayed as formed caspase-3 from procaspase-3 in the S-100. Caspase-3 activity without addition of cytochrome *c* was used as the negative control.

2.2.3. Administration method of D-galactosamine and tea-catechin derivatives in rats. Liver apoptosis was induced according to Muntane's method, by intraperitoneal injection of D-galactosamine [3,4]. A single dose of D-galactosamine was administered intraperitoneally

*Corresponding author. Fax: +81 88 622 2503.
E-mail address: katunuma@tokushima.bunri-u.ac.jp (N. Katunuma).

Abbreviations: AST, aspartate aminotransferase; ALT, alanine aminotransferase; EGCG, epigallo-catechin gallate; ECG, epi-catechin gallate; CG, catechin gallate; EC, epi-catechin; EGC, epigallo-catechin; C, catechin; GC, gallo-catechin; G, gallate; LPS, lipopolysaccharide; TdT, terminal transferase; MCA, methyl coumaryl amide

0014-5793/$32.00
doi:10.1016/j.febslet.2005.12.087

(0.5 g/kg), and rats were sacrificed 12 h after the injection. Two doses of EGCG with 50 μg/kg of LPS were administered intraperitoneally at 1 h before and after the D-galactosamine administration. EGCG was further administered twice at 3-h intervals.

2.2.4. Preparation of liver cytoplasm for assay of caspase-3 activity. Liver cytoplasm fraction for caspase-3 activity assay was prepared by sequential centrifugation method for cell organelle separation according to a method described by Fleisher and Kervina [16].

2.2.5. TdT-mediated dUTP nick end labeling (TUNNEL) assay. Apoptotic cells were detected in sections using the in situ Apoptosis Kit (Takara Kyoto, Japan). Frozen sections of liver tissues were fixed in 3% paraformaldehyde, incubated with protease K (20 μg/ml) for 10 min, and then presoaked in terminal transferase (TdT) buffer (0.5 μM/L cacodylate, 1 μM/L CoCl, 0.5 μM/L dithiothreitol, 0.05% bovine serum albumin, and 0.15 M/L NaCl) for 10 min. Sections were incubated for 1 h at 37 °C in 25 ml of TdT solution, containing 1× terminal transferase buffer, 0.5 nM of biotin-dUTP, and 10 U of TdT. After the TdT reaction, sections were soaked in TdT blocking buffer (300 nM/L NaCl and 30 mM/L tri-sodium citrate-2-hydrate), incubated with HRP-conjugated streptavidin for 30 min at room temperature, and developed for 10 min in phosphate-buffered citrate (pH 5.8) containing 0.6 mg/ml DAB. Nuclei were counterstained with hematoxylin.

3. Results

3.1. Inhibition of caspase-3 activity by various catechin derivatives in vitro

Caspase-3 plays a central role as an executive enzyme of apoptosis in the final step of various apoptotic cascades [5–9].

Table 1
Comparison of inhibition of caspase-3 activity in vitro and the apoptosis test using cultured HeLa cells by tea-catechin derivatives

Catechin Derivatives	*in vitro* 50% Inhibition of caspase-3	HeLa cell apoptosis test 50% inhibition of apoptosis test
Epigallo-Catechin Gallate 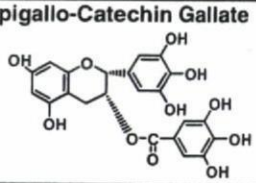	1×10^{-8} M	1×10^{-6} M
Epi-Catechin Gallate 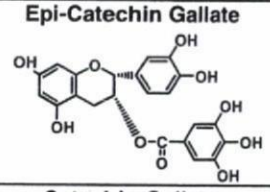	1×10^{-7} M	1×10^{-4} M
Catechin Gallate 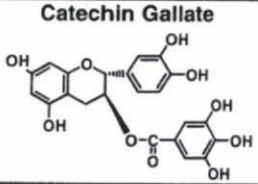	1×10^{-6} M	5×10^{-4} M
Epigallo-Catechin 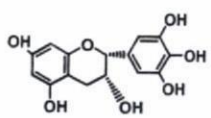	1×10^{-6} M	5×10^{-4} M
Epi-Catechin 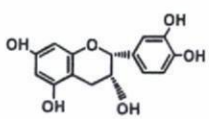	1×10^{-6} M	5×10^{-4} M
Catechin Gallate 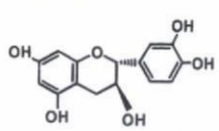	Gallo-Catechin 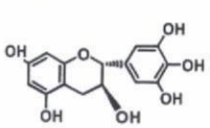	Gallic Acid 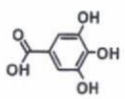	No Inhibitions by 1×10^{-4} M

The left-hand column shows the concentrations of catechin derivatives inducing 50% inhibition of caspase-3 activity in vitro. The right-hand column shows the 50% inhibition of the apoptosis test units of cultured HeLa cells. The assay methods are described in the text [10,11]. The 50% inhibition concentrations of various catechin derivatives are illustrated ($n = 3$, the mean ± S.E.M. with $^{*}P < 0.01$).

Caspase-3 activity was completely inhibited by EGCG at 1×10^{-7} M and was inhibited to 50% at 1×10^{-8} M in vitro. Epi-catechin gallate (ECG) showed 50% inhibition at 1×10^{-7}M, and catechin gallate (CG), epi-catechin (EC) and epigallo-catechin (EGC) had induced inhibition at 1×10^{-6} M. Catechin (C), gallo-catechin (GC) and gallate (G) showed no inhibition as Table 1 shows. The stereo-binding form of –OH to the catechin-ring should be an epi-structure to display inhibitory activity. The presence of either component, catechin gallate (CG) and/or epi-form catechin (EC), is essential.

Relationship of velocity and substrate concentration of caspase-3 in the presence of EGCG showed a typical sigmoidal curve and the Lineweaver–Burk relationship did not give a straight line, but showed a logarithmic curve. When the abscissa was taken as $1/[S]^2$, the logarithmic curve changed to a straight line (Fig. 1A). The inhibition kinetics of these catechin derivatives appear to be a 2nd-order sigmoidal allosteric inhibition as follows:

$$1/v = Km/V(1/[S]^2) + 1/V.$$

The other four effective catechin derivatives, such as ECG, CG, EC and EGC, also showed the same type of allosteric inhibition to caspase-3 as that by EGCG (figures are abbreviated).

The binding site of the catechins appeared to be different from the substrate-binding site. The allosteric nature of caspase-3 using synthetic inhibitors was reported by Hardy et al. [11] (see Section 4). The molecular weight of caspase-3 did not appear to change in the presence of EGCG and/or substrate using Superdex G-75. Therefore, polymerization or depolymerization was not observed using these allosteric inhibitors (data not shown).

3.2. Inhibitions of activities of caspases-7 and 2 activities by EGCG in vitro

Caspases-7 and 2 are also known to participate in various apoptosis cascades. The activities of caspases-7 and 2 were also strongly inhibited by EGCG, and the 50% activities were inhibited at 1×10^{-6} M. However, the mode of inhibitions of caspases-7 and 2 were different from that of caspase-3. The V_{max} decreased in the presence of EGCG and the Lineweaver–Burk relationship showed a non-competitive type inhibition (Fig. 1B and C). The binding site to EGCG is the same as the substrate-binding site or located near the active site. Caspase-8, cathepsins B and L, which are the same cysteine proteases, were not inhibited at 1×10^{-5} M of EGCG. Therefore, the inhibitions of caspases are not due to an attack to the active site –SH of these enzymes by the scavenger effect of catechins.

3.3. Inhibition of caspase-3 in HeLa cell apoptosis test induced by cytochrome c by EGCG

Wells et al. developed a cell-free apoptosis test using cultured HeLa cells [12]. The S-100 prepared from cultured HeLa cell cytoplasm contains sufficient amounts of procaspase-3 and the activating enzyme system except cytochrome *c*. Caspase-3 activity in the S-100 increased following the addition of cytochrome *c*, as shown in Fig. 2. The 70% of the apoptosis unit was inhibited by EGCG at a concentration of 1×10^{-5} M. The strengths of suppression by the various catechin derivatives were in the same order as the inhibitions of caspase-3 activity in vitro, as shown in Table 1.

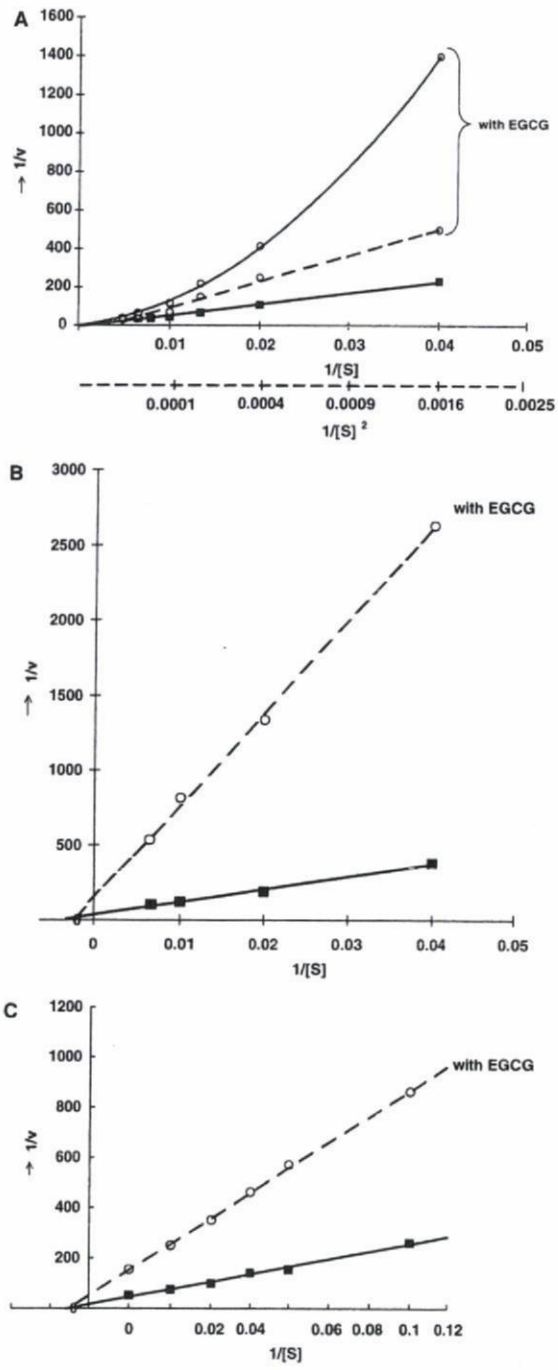

Fig. 1. Mode of inhibitions of caspase-3, 2 and 7 by EGCG in Lineweaver–Burk relationship. (A) Caspase-3 inhibition by 1×10^{-7} M of EGCG. The $1/v$ values to the $1/[S]$ in the presence of EGCG are expressed as open circles with a thin solid line (○–○). The $1/v$ values to the $1/[S]$ in the absence of EGCG are illustrated as closed squares with a solid line. The $1/v$ values to the $1/[S]^2$ illustration in the presence of EGCG are expressed as open circles with a broken line (○---○). (B) and (C) Caspase-2 or 7 inhibition by 1×10^{-6} M of EGCG. The activities in the absence of EGCG are illustrated as solid line with a solid line and the activities in the presence of EGCG are illustrated as open circles with a broken line. (B) shows caspase-2 inhibition by EGCG; the Lineweaver–Burk relationship. (C) shows caspase-7 inhibition by EGCG. All symbols and lines are the same as those in (B).

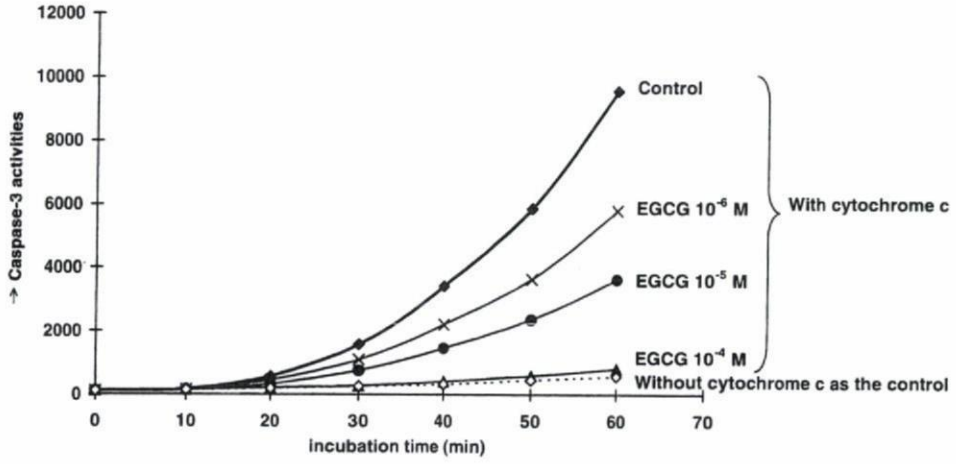

Fig. 2. Inhibition of caspase-3 activities in apoptotic test using cultured HeLa cells induced by cytochrome *c* by EGCG. Caspase-3 inhibition in S-100 of cultured HeLa cells by various catechin derivatives was assayed using Nguyen and Wells' apoptosis test as shown in Table 1, right panel [12]. The inhibitory activities by various catechin derivatives are compared as 50% inhibition concentrations as shown in Table 1, in left panel. The catechin derivatives added were expressed as the final concentrations in the S-100 fraction. All data are the means ± S.E.M. ($n = 5$) with $^{*}P < 0.01$.

3.4. Liver apoptosis induced by D-galactosamine plus LPS, and its prevention by EGCG in vivo

Sufficient amounts of procaspase-3 are present and active caspase-3 is not present in the normal hepatocyte cytoplasm. However, procaspase-3 in the cytoplasm is activated to form active caspase-3 by the effective apoptotic signal. It is well known within the pathological field that hepatocyte injury induced by D-galactosamine results in hepatocyte apoptosis, as assessed by the TUNNEL-staining and the DNA ladder formation [3,4,10].

(1) Elevations of liver caspase-3 activity and serum aminotransferases in D-galactosamine induced hepatocyte apoptosis, but were prevented by cotreatment with EGCG, as shown in Table 2. The both elevations were prevented by cotreatment with EGCG in a dose-dependent manner, and treatments with 50 mg/head EGCG suppressed the activity to the normal level. Furthermore, the macroscopic liver profile was protected and resembled to normal level.

However, the mechanism of procaspase-3 activation cascade induced by D-galactosamine remains unknown (see Section 4).

(2) TUNNEL-staining method, which is the most established DNA nick formation in the nucleus, was examined in these livers. As shown in Fig. 3, the significant nick staining of nuclear DNA was observed in the livers treated with D-galactosamine, while nick formations was significantly suppressed by cotreatment with EGCG. These data show that D-galactosamine induced liver injury resulted in caspase-3 mediated apoptosis and the apoptosis was significantly suppressed by EGCG administration.

(3) Increased activities of AST and ALT in the serum by D-galactosamine administration, which are the established marker for hepatocyte injury, were also completely suppressed by cotreatment with EGCG dose-dependently as shown in Table 2. EGCG showed an effective protecting effect for the liver injury mediated by caspase-3.

4. Discussion

There are several papers on cancer prevention by tea-catechin derivatives, which appear to contradict our own data.

Table 2
Elevation of caspase-3 activities in rat liver cytoplasm in vivo and the activities of AST and ALT in the serum following D-galactosamine administration, and the preventions by EGCG treatment in vivo

	Caspase-3 activities in liver (AFC nM/mg/h)	Aminotransferases in serum (IU/l)	
		AST	ALT
Control LPS	<100	<37.8	<5.8
D-GalN	1000.0	450.0	300.0
D-GalN + LPS	5500.0	5229.3	1438.3
D-GalN + LPS + EGCG 10 mg	3500.0	–	–
D-GalN + LPS + EGCG 30 mg	300.0	320.5	114.0
D-GalN + LPS + EGCG 50 mg	100.0	<100	<100

0.5 g/kg D-galactosamine with 50 μg/kg LPS was administered once intraperitoneally. The D-galactosamine administration method and the preparations of the liver cytoplasm for the caspase-3 assay are described in Section 2.2. The injection doses of EGCG are mg/head. Elevation of caspase-3 activities in the liver cytoplasm in D-galactosamine-induced apoptosis and the preventions by EGCG are in the left columns. The dose-dependent suppressions of caspase-3 activities by EGCG administration are represented in the left columns. All data represent the means ± S.E.M. ($n = 5$) with $^{*}P < 0.01$.

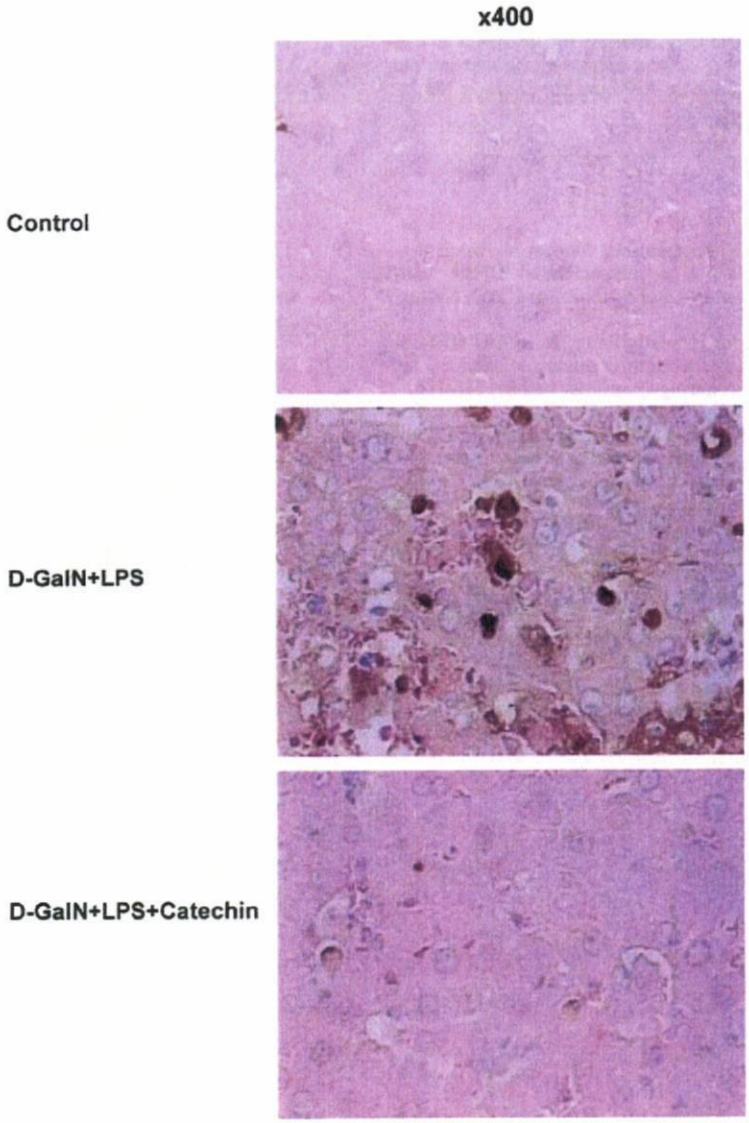

Fig. 3. Hepatocyte apoptosis images using TUNNEL-staining induced by D-galactosamine plus LPS and its prevention by EGCG cotreatment. Th staining method is described in Section 2.2. These images are 400× magnification. Top image shows the control liver, the middle image shows live administrated D-galactosamine plus LPS and the suppression profile by EGCG is shown in the bottom image.

However, this is completely different phenomenon from the following reasons; the reported effective concentration of catechin for cancer prevention is very high 10^{-3}–10^{-4} M [13], these concentrations are not physiological and appear to be toxic concentration. On the other hand, inhibition of caspase-3 by catechins was 10^{-6}–10^{-7} M in vitro and in vivo. Furthermore, these papers do not mention on the relationship between cancer cell death and apoptosis mediated by caspases [13–15]. Some papers reported that catechin stimulates release of TNF-α and enhances effect of anticancer drugs in vivo. While there is data demonstrating the prevention of oncogenesis in vivo, there is no research at the molecular level [14,15].

There are two possible mechanisms by which catechin suppresses hepatocyte apoptosis induced by D-galactosamine administration. One is due to direct inhibition of caspase-3 activity and the other is due to elimination of O_2^-, which is produced by D-galactosamine-protein binding through Maillar reaction. Both mechanisms are likely.

Caspase-3 is constructed from a heterotetramer, which i composed of two pairs of heterodimers. Each unit is compose of a long chain and a short chain. The substrate-binding site i located in the long chains. The interaction between the lon chain and short chain and also the unit-to-unit interaction are susceptible to allosteric effectors. For example, it has bee reported by Hardy et al. [11] using synthetic allosteric inhib tors that the inhibitor-binding site of the caspase-3 molecul is different from the substrate binding site. They also reporte that the –SH of these inhibitors can form a disulfide bond wit the cysteine-SH at amino acid 290th of the enzyme, which i different from the active site cysteine in the long chain. Th practical conformational change by EGCG will be made clea using X-ray co-crystallography.